The Journal of Chemical Physics

Concave polymer brushes inwardly grafted in spherical cavities: A Molecular Dynamics study

Cite as: J. Chem. Phys. (in press) (2023); https://doi.org/10.1063/5.0141450
Submitted: 05 January 2023 • Accepted: 13 February 2023 • Accepted Manuscript Online: 13 February 2023

Andrey Ivanov Milchev and Peicho Petkov

Accepted to J. Chem. Phys. 10.1063/5.0141450

Concave polymer brushes inwardly grafted in spherical cavities

Andrey Milchev*,† and Peicho Petkov‡

†*Institute of Physical Chemistry, Bulgarian Academy of Sciences, 1113 Sofia, Bulgaria*

‡*Sofia University St. Kliment Ohridski, Physics Dept., Sofia, Bulgaria*

E-mail: milchev@ipc.bas.bg

Abstract

The structure and scaling properties of inwardly curved polymer brushes, tethered under good solvent conditions to the inner surface of spherical shells like membranes and vesicles, are studied by extensive Molecular Dynamics simulations and compared with earlier scaling and Self-Consistent Field Theory (SCFT) predictions for different molecular weight of the polymer chains N and grafting density σ_g in the case of strong surface curvature, R^{-1}. We examine the variation of the critical radius $R^*(\sigma_g)$, separating the regimes of *weak concave brushes* and *compressed brushes*, predicted earlier by Manghi et al.[Eur. Phys. J. E **5**, 519 (2001)] as well as various structural properties as the radial monomer- and chain-end density profiles, orientation of bonds, brush thickness, etc. The impact of chain stiffness, κ, on concave brush conformations is briefly considered too. Eventually we present the radial profiles of local pressure normal, P_N, and tangential, P_T, to the grafting surface, the surface tension $\gamma(\sigma_g)$, for soft and rigid brushes, and find a new scaling relationship $P_N(R) \propto \sigma_g^4$, independent of the degree of chain stiffness.

1 Introduction

During recent years there has been strong interest in the properties and functional behavior of polymer brushes, i.e., in films comprised of end-tethered chains as promising surface coatings and materials of the future relevant for a broad variety of applications[1]. Different aspect of polymer science and technology ranging from medical and bilogical applications[1–5], flow valving[6,7], or responsive devices[8] have lead therefore to intensive research and produced an impressive headway in the understanding and application of such materials. While originally most of experimental and theoretical investigations of such coatings have been focused on studies of polymer brushes anchored to planar surfaces[9–12], more recent scientific interest has been focused on brushes on curved (both concave and convex) interfaces in view of their wide scale applications in drug delivery[13], oil recovery[14], emulsion stabilization[15], superhy-

drophobic coatings[16], etc. In this context numerous theoretical studies based on different approaches such as scaling analysis, Density Functional- (DFT) and Self-Consistent Field Theory (SCFT) as well as Monte Carlo and Molecular Dynamics simulations[17,18,21] have shed much insight into many aspects regarding the structure and behavior of such polymer brushes. Triggered by the classical work of Daoud-Cotton[19], where the use of scaling analysis based on the notion of blobs has produced a faithful description of flexible chains tethered to convex surfaces, many such studies have been dedicated to the exploration of convex polymer brushes[20–22] while concave brushes have been considered mainly as tethered to the inner surface of cylindrical pores[23–30].

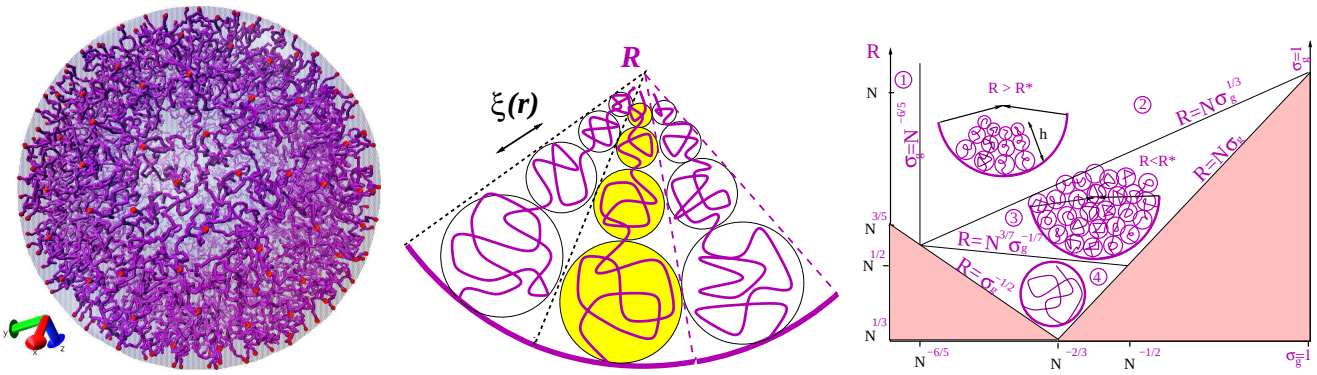

Figure 1: (left) A snapshot of a concave brush with chain length $N = 64$ in a spherical shell with radius $R = 48.5$ at grafting density $\sigma_g = 0.010$. (middle) Conformation of a concave brush with blob size $\xi(r)$ for $R = R^*$ in an inverted Daoud-Cotton description. (right) Different regimes for an inwardly grafted brush in a spherical cavity with radius R at grafting density σ_g and chain length N, according to Manghi et al.[31]

Regarding the structure and stability of concave brushes grafted to the inner surface of spherical cavities, Fig.1a, it has been first the important work of Manghi et al.[31] who employed SCFT and scaling analysis so as to demonstrate that generally, "concave is not like convex", and that using an inverted version of the classical Daoud-Cotton scaling approach, Fig.1b, has lead to unphysical results in previous theoretical considerations. In particular, it has been shown[31] that for weak curvature, $R > R^*$, when the sphere radius R exceeds a critical value $R^* \approx 1.3h_{plan}$ with h_{plan} being the thickness of a planar brush with the same grafting density σ_g, inwardly curved brushes behave qualitatively like flat brushes. In

contrast, for strong curvature, $R < R^*$, the monomer concentration becomes progressively uniform as one moves from the grafting surface toward the cavity center like in a semi-dilute solution of uniform concentration. The various regimes for an inwardly grafted spherical brush have been presented in a phase diagram[31], Fig.1c, in terms of the number of monomers per chain N and the grafting density, σ_g, for arbitrary inverse curvature $1/R$. To the best of our knowledge, however, there have been no attempts to test and verify these theoretical predictions[31] by means of computer experiments. An earlier study by means of lattice Monte Carlo simulations[32] considered the average segment densities of tethered chains in a cavity and demonstrated that the density of segments, $\rho(r)$, is largely constant as reported by early experimental work[33]. Therefore, in this work we present a comprehensive investigation of such concave polymer brushes by means of Molecular Dynamics simulations focusing on the most important regimes 2 and 3 of the phase diagram, Fig.1c, in an attempt to test and verify the findings from our computer experiments with the theoretical predictions[31]. In addition, we examine the impact of chain stiffness on the structure of inwardly grafted concave brushes and determine the radial profiles of the local pressure in a spherical cavity.

2 Model Details and Aspects of the Simulation Method

We use a coarse-grained description for the segments, representing each chain molecule simply by a bead-spring model, i.e., a sequence of N effective spherical monomeric units held together by suitable effective potentials. Any pair of beads (i, j) in the system at distance $r = |\vec{r}_i - \vec{r}_j|$ interacts with the purely repulsive Weeks - Chandler - Andersen (WCA) potential[34],

$$V^{WCA}(r) = \begin{cases} 4\epsilon[(\sigma/r)^{12} - (\sigma/r)^6 + 1/4] + \epsilon, \ r < r_c = 2^{1/6}\sigma, \\ 0, \ r > \sigma 2^{1/6}. \end{cases} \quad (1)$$

Here ϵ sets the scale for the strength of this potential, σ is the range, and we choose units of energy and length such that $\epsilon = 1$ and $\sigma = 1$. Note that as solvent particles are not explicitly included, the lack of any attractive part in Eq.(1) means that we restrict attention to very good solvent conditions. A typical configuration of an inwardly bent concave polymer brush is shown in Fig.1a for a capsule with radius $R = 48.5\sigma$ and number of beads per chain $N = 64$ at grafting density $\sigma_g = 0, 10$.

The connectivity of the chain molecule is maintained by applying the "finitely extensible nonlinear elastic" (FENE) potential[35] between effective monomers which are nearest-neighbors along a chain,

$$V^{FENE}(r) = \begin{cases} -0.5\, k\, r_0^2\, \ln[1-(r/r_0)^2],\ r < r_0, \\ \infty,\ r > r_0, \end{cases} \tag{2}$$

choosing the constants k, r_0 as usual[35]: $k = 30\epsilon/\sigma^2$ and $r_0 = 1.5\sigma$. With this choice, the nearest-neighbor distance between beads along the chain then is $l_b \approx 0.976$ (at a temperature $k_B T = 1$).

The stiffness of the polymer chains is controlled by a bond bending potential chosen as

$$U_b(\theta_{ijk}) = \kappa[1 - \cos(\theta_{ijk})] \tag{3}$$

where θ_{ijk} is the bond angle formed between the two subsequent unit vectors along the bonds connecting monomers i with j, and j with k, respectively. For flexible chains one has $\kappa = 0$ while the degree of rigidity of semiflexible chains is characterized by their persistence length $\ell_p \approx \kappa$ for $\kappa/k_B T \geq 2$.[36] and the ratio of ℓ_p to the chain's contour length, $(N-1)\sigma$.

Finally, the confinement by a rigid spherical surface is also described by Eq. (1), where r is replaced by $z = R - r$, *i.e.*, the normal distance from the sphere surface in the direction towards its center. Note that we do not assume any dependence of this wall potential on the radius R of the sphere. A clear advantage of our model is that in the limit $R \to \infty$ it

reduces to the case of a brush on a planar substrate. For the Molecular Dynamics (MD) simulations[37], the HOOMD-blue software package for graphical processing units (GPUs) is used[39,40].

Newton's equations of motion are numerically integrated using the standard velocity-Verlet algorithm[37]. Using units such that effective monomers have mass $m = 1$, the MD time unit $\tau_{MD} = \sqrt{m\sigma^2/\epsilon} = 1$, and using an integration time step $\Delta t = 0.05$, observation times of $10^7\tau_{MD}$ can be reached, keeping the temperature constant by means of a Langevin thermostat with a friction coefficient of 2.0.

Originally, for the creation of the concave brush an appropriate number of beads, M, is placed at random on the spherical surface so that the mean distance among them is of the order of a bond length, $4\pi R^2/M \approx 2^{1/6}\sigma$. The system of such beads is then equilibrated using long-ranged Coulomb repulsive forces in order to achieve a nearly equidistant positions to be used as grafting points for the polymer chains. Alternatively, we also employed the Matlab S^2-Sampling Toolbox[38] to generate a nearly uniform triangular tessellation of M points on the spherical shell with radius R. Then a subset of $M' < M$ equally spaced points is chosen and used as anchoring sites for the M' polymer chains forming the brush so that $\sigma_g = M'/(4\pi R^2)$. Each of the M' chains is taken at first as a stiff rod comprised of N beads connected by bonds with 25% reduced bond length. Such chains are then inserted *radially* into the capsule at each anchoring site on the spherical surface. This starting configuration is then equilibrated by using soft Gaussian repulsive forces between the monomers, $U_{Gauss}(r) = \epsilon \exp\left[\frac{1}{2}\left(\frac{r}{\sigma}\right)^2\right]$. In the course of the equilibration procedure the partially overlapping monomers attain gradually their full excluded volume whereby the Gaussian potential is successively replaced by a stiffer Morse potential, $U_{Morse}(r) = \varepsilon(\exp\left[-2\beta(r-\sigma)\right] - 2\exp\left[-\beta(r-\sigma)\right])$ with $\beta = 3.0$ and the bonds being given their final length. Eventually the Morse potential is replaced by the WCA potential, Eq.(1). The equilibration is considered finished after typically 2×10^7 integration steps so that no changes in the resulting monomer density profile can be detected.

In the course of the simulations we determine the radial density distribution of monomers, $\rho(r)$, the distribution of chain ends, $\rho_e(r)$, the height h of the concave brush as well as the orientation of polymer bonds, $\eta(r)$, and that of the chain end-to-end vectors, $\eta_E(r)$, with respect to the radius vector pointing to their respective mid-point positions. Here

$$\eta(r) = \frac{3}{2}\langle \cos(\theta(r))^2 \rangle - \frac{1}{2}, \tag{4}$$

where $\theta(r)$ denotes the angle between the bond vector and the radius vector to the bond mid-point. Thus, $\eta = 1$ and $\eta \approx -0.5$ indicates bonds oriented along or perpendicular to the radius vector while $\eta \approx 0$ stands for randomly oriented bonds.

The local pressure profiles along $\vec{e}_N$-direction within a spherical slice $\Re$ between two spheres with radii R_- and R_+, where $\Re = \{R_- \leq |\vec{r}| \leq R_+\}$, with volume $|\Re| = 4\pi(R_+^3 - R_-^3)/3$ can be determined as[41]

$$P_N(\Re) = \frac{1}{|\Re|}\int_{\Re} d\vec{r} \int_C (d\vec{l}.\vec{e}_N)(\vec{F}.\vec{e}_N)\delta(\vec{r} - \vec{l}), \tag{5}$$

$$P_T(\Re) = \frac{1}{2|\Re|}\int_{\Re} d\vec{r} \int_C (d\vec{l} \times \vec{e}_N)(\vec{F} \times \vec{e}_N)\delta(\vec{r} - \vec{l}) \tag{6}$$

Here $\vec{e}_N, \vec{e}_T$ denote orthonormal vectors, $\vec{F}$ is the force including both pair non-bonded, Eq.(1), and bond stretching forces, Eq.(2), as well as non-pairwise angle-bending forces, Eq.(3), acting between particles. C stands for the integration contour connecting these particles whereby in a spherical system one selects $\vec{e}_N = \vec{r}/r$. The surface tension γ is given by the expression suggested by Lovett[42,43]

$$\gamma = \int_0^\infty dr[P_N(r) - P_T(r)]. \tag{7}$$

Accepted to J. Chem. Phys. 10.1063/5.0141450

3 Results

3.1 Structure and scaling of inwardly grafted soft polymer brush

In this section we consider inwardly grafted brushes comprised of entirely flexible polymers with different chain length N and grafting density σ_g, placed within an impenetrable spherical shells of radius $R = 24.5$ and $R = 48.5$. In Fig.2a we show the radial density profiles for a series of flexible polymer chains, $\kappa = 0$, with length $16 \leq N \leq 64$ at grafting density $\sigma_g = 0.11$, tethered to a shell with radius $R = 48.5$. For $N = 64$ and $\sigma_g = 0.11$ the sphere is entirely filled up by the brush with the brush tip just reaching the sphere center so that in this case R attains the critical value R^*, according to Ref.[31]. Therefore, for $N \leq 64$ the system is in the regime 2 of *weak concave brushes*, $R > R^*$, see Fig.1c. The pronounced oscillations of $\rho(r)$ in the vicinity of the confining wall, i.e., around $r = 48.5$, seen in Fig.2 a, Fig.2c, Fig.3a-d, indicate that the positions of the first monomers immediately next to the anchoring site remain nearly constant with negligible fluctuations during the simulation due to the immobile roots of the brush chains and the lack of interactions with beads from neighboring chains whose roots are rather far. A similar effect at the center of the cavity can be observed in Fig.8h for $\sigma_g = 0.17$ where the high density of monomers along with the chain stiffness lead to nearly crystalline packing and immobilization of the monomers at the origin. Apparently, the radial distributions of monomers, $\rho(r)$, follow a typical profile vanishing with a tail, similar to that of polymer brushes on planar substrates, which deviates as expected from the purely parabolic shape, cf. Fig.2a (dashed line), predicted by the SCFT[31]. Regarding the latter, one should note the work of Amoskov *et al.*[45] who elaborated the SCF approach and showed that for $\rho(r) > 0.1$ the density profile is parabolic, for $\rho(r) > 0.5$ it is flattened, and for $\rho(r) > 0.8$ the density profile is nearly step-like.

Fig.2b shows the corresponding distributions of chain ends within the sphere. The inset in Fig.2b displays the variation of the height $h(N)$ with growing length N whereby a deviation above $N \approx 40$ from the linear scaling with N typical for planar brushes is clearly evident.

Accepted to J. Chem. Phys. 10.1063/5.0141450

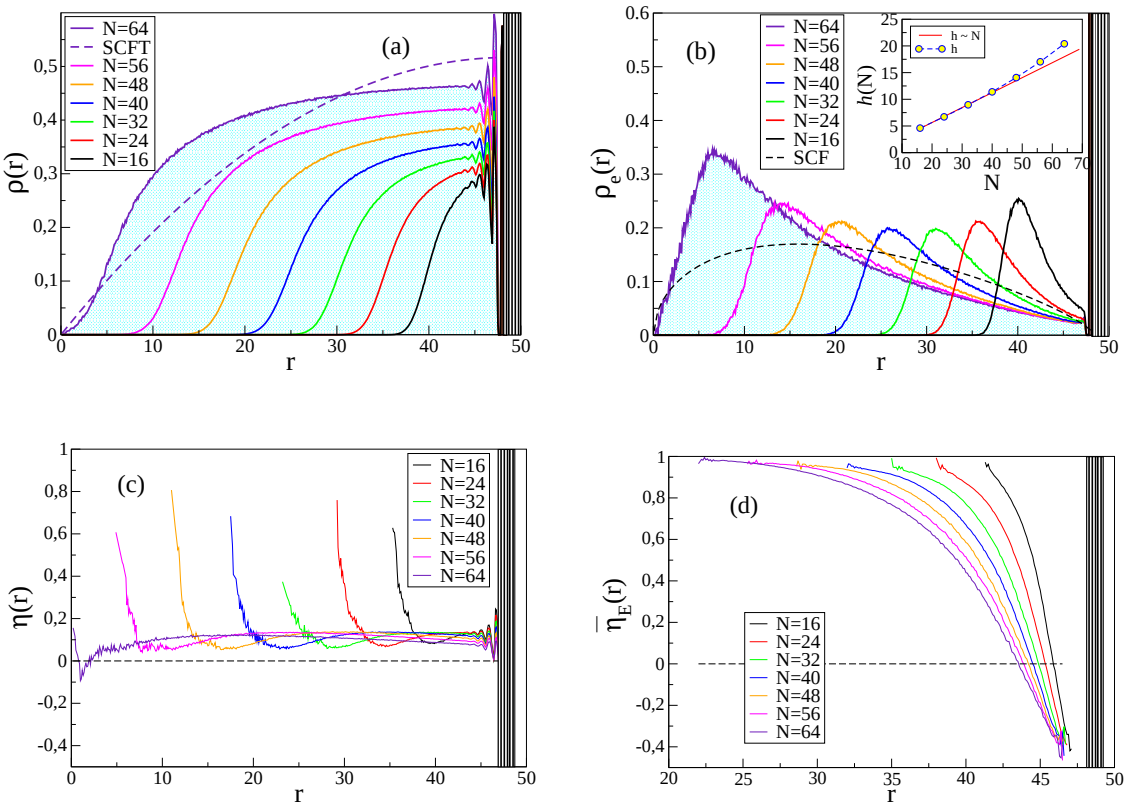

Figure 2: (a) Radial density distribution $\rho(r)$ for different chain length N at grafting density $\sigma_g = 0.11$ and sphere radius $R = 48.5$. For $N = 64$ one has $R = R^*$. Dashed line denotes the SCFT result[31] for $R = R^*$. (b) Radial distribution of the chain ends, $\rho_e(r)$. The inset shows the variation of the brush height $h(N)$ with $N \leq 64$. (c) Radial distribution of bond orientation $\eta(r)$ for different chain length N at grafting density $\sigma_g = 0.11$ and sphere radius $R = 48.5$. (d) The same as in (c) but for the end-to-end vectors orientation, $\eta_E(r)$.

Thus, the impact of shell curvature leads to significant deviations in the scaling laws for concave brushes in comparison to brushes on planar substrates already in regime 2. For $N = 64$, that is, when $R = R^*$ for the chosen $\sigma_g = 0.11$, the height of the concave brush exceeds that of a planar brush by $\approx 11\%$ while the onset of deviation begins at $r \geq 0.8R^*$.

The orientation of bonds $\eta(r)$ with respect to the radius vector from the cavity center to the mid-bond position, Fig.2c, at $\sigma_g = 0.11$ indicates that radially oriented bonds along the chain backbone slightly prevail over randomly oriented ones, $\eta(r) \approx 0.1$, except at the top of the brush where owing to confinement bonds increasingly orient radially thus maximising entropy due to increased steric repulsion. In contrast, the end-to-end vector orientation of chains, $\bar{\eta}_E(r)$, plotted against the chain's center of mass position, r, is almost entirely

radially oriented, see Fig.2d, except for few polymer chains in the vicinity of the spherical shell whereby this tendency increases with growing chain length N.

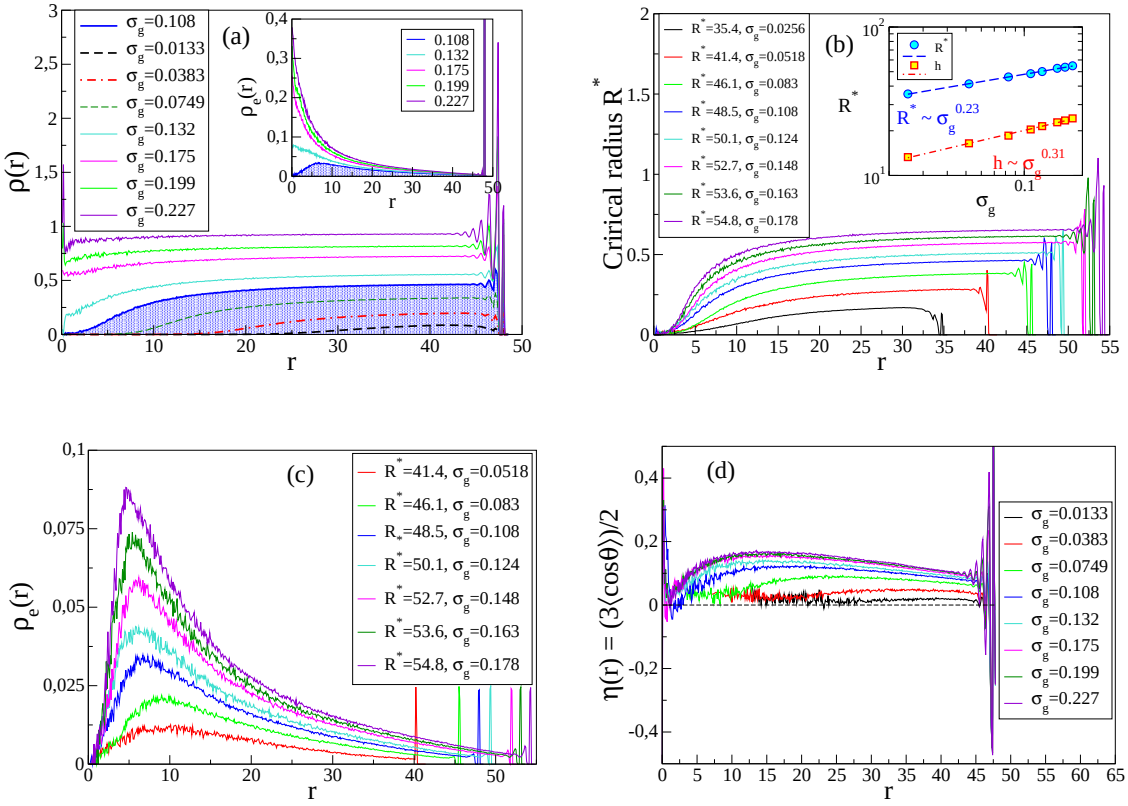

Figure 3: (a) Radial density profiles $\rho(r)$ for different grafting density σ_g at fixed sphere radius $R = 48.5$ and $N = 64$. A thick blue line on top of a shaded area underneath denotes the 'critical' case for $\sigma_g = 0.108$ which yields $R^* = 48.5$. (b) Density profiles $\rho(r)$ for chains with $N = 64$, corresponding to different $R^*(\sigma_g)$ as indicated. The scaling of R^* with σ_g yields an exponent $\alpha \approx 0.23 \pm 0.01$, while the brush thickness $h \propto \sigma_g^{1/3}$ as expected[44], see inset. (c) The same as in (b) but for the radial distribution of chain ends $\rho_e(r)$. (d) Radial orientation of bonds.

The change in the radial density profiles $\rho(r)$ in a cavity of radius, $R = 48.5$, with growing grafting density σ_g is shown in Fig.3a which demonstrates that the critical radius $R^* = 48.5$ is reached here for $\sigma_g = 0.108$ whereas denser concave brushes beyond this value of σ_g are compressed, indicating a uniform density distribution as expected for the regime 3, cf. Fig.1. In fact, Fig.3b demonstrates that beyond R^* (i.e., for $\sigma_g \geq 0.108$) the monomer concentration throughout the sphere becomes progressively uniform featuring a compressed semidilute

polymer solution where monomer-monomer repulsion prevails over chain stretching. The distribution of chain end-monomers, shown in the inset of Fig.3a, demonstrates a rapidly growing maximum at the center of the spherical cavity as the grafting density becomes larger, $\sigma_g > 0.108$, $r = 0$, in agreement with the SCFT predictions[31]. In particular, for $\sigma_g = 0.178$ one has $R/R^* = 0.885$, cf. inset in Fig.3a, whereby the end-monomer distribution resembles the SCFT result of Fig.5 in Ref.[31].

Apparently, one could vary systematically the shell radius, R, at fixed length of the polymer chains, N, and an arbitrary chosen grafting density σ_g until the tip of the density profile, $\rho(R)$, touches the sphere center and thus determine the critical radius, R^*, which separates the regimes of weak concave brushes, 2, from that of compressed brushes, 3, for the resulting σ_g, see Fig.3b. In such "critical" cases $R = R^*$, cf. Fig.3b, the distributions of chain ends, Fig.3c, reveal a well expressed maximum which gradually approaches the cavity center with growing R^*. For the system in Fig.3c this maximum is seen to move gradually inwards from $r \approx 9.5$ for $\sigma_g = 0.052$ to $r \approx 4.6$ for $\sigma_g = 0.178$. The position r^e_{max} of $\rho_e(r)$, Fig.3, approaches the cavity center as $r^e_{max} \approx 1.95\sigma_g(R^*)^{-0.56}$.

One may check one of the basic scaling predictions regarding the phase boundary between weak and compressed concave brushes, expected to scale as $R^*(\sigma_g) \propto \sigma_g^{\alpha} N$ with $\alpha = 1/3$, according to SCF theory[31]. Notably, as shown in the inset of Fig.3b, our numerical data yield for $N = 64$ a scaling exponent $\alpha \approx 0.23$ which is smaller than the theoretically predicted value of $\alpha = 1/3$ valid for $N \to \infty$, $R \to \infty$. This finding can be interpreted certainly as a typical finite-size effect, given that the scaling predictions[31] are supposed to be valid in the asymptotic limit $N \to \infty$, $R \to \infty$. Apparently, even though α is found to grow gradually with N, Fig.4a, the chain lengths feasible in our MD simulations are still far from the asymptotic values considered by the SCF theory. Yet, the observed deviation of $h(N)$ from the planar scaling, $h_{plan} \propto N$, cf. Fig.4b, suggests that shell curvature exerts a significant impact on the structure of concave brushes long before the boundary of region 2 is reached. Therefore, in Fig. 4a we examine the variation of the scaling exponent α

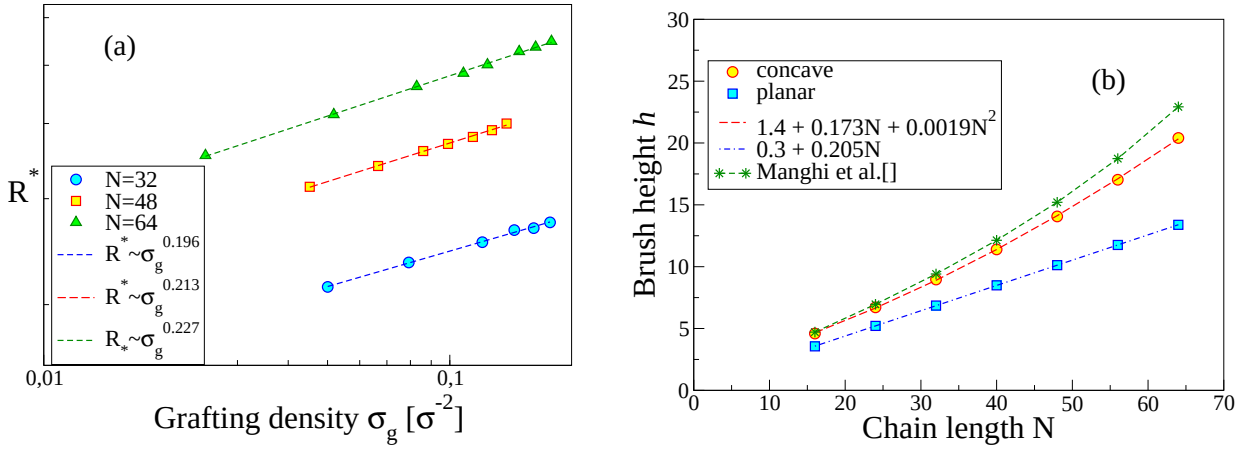

Figure 4: (a) Scaling of the critical radius R^* with grafting density σ_g for several concave brushes of chain lengths N. (b) Variation of brush height $h(N)$ with N for $R = 48.5$ and $\sigma_g = 0.11$ in the case of concave and planar substrate as indicated. Dashed lines denote extrapolations of the observed results.

several systems of inwardly curved brushes of polymer chains with length $N = 32, 48, 64$ where the exponent α gradually approaches $1/3$ with increasing R^*. Yet, it suggests that $\alpha = 1/3$ would be reached for chains with $N \approx 400$. In Fig.4b we compare the change of brush height (thickness) $h(N)$ with N in the regime $R > R^*$. Apparently, while the height of brushes on planar substrate is confirmed to grow linearly with increasing N, in agreement with theoretical predictions, the height of an inwardly curved brush in region 2 deviates markedly from a linear growth. In fact, our simulational results reveal a quadratic variation of h with N, and thus agree narrowly with the suggested asymptotic relationship, Eq.(25)[31], predicted for the ratio $h(R)/h_{plan}(R)$ (with h_{plan} denoting the height of a planar brush) in region 2 for the case of weak curvature.

The difference between planar and concave brushes is particularly well expressed if one compares the distribution of the total number of monomers, $N_{tot}(r)$, in a slice of thickness $r + \Delta r$ at distance r from the grafting surface. This is shown in Fig.5a for a series of chain lengths, N, at given grafting density $\sigma_g = 0.11$. Evidently, for weak curvature a concave brush contains much less repeat units at distance r from the grafting surface than a planar

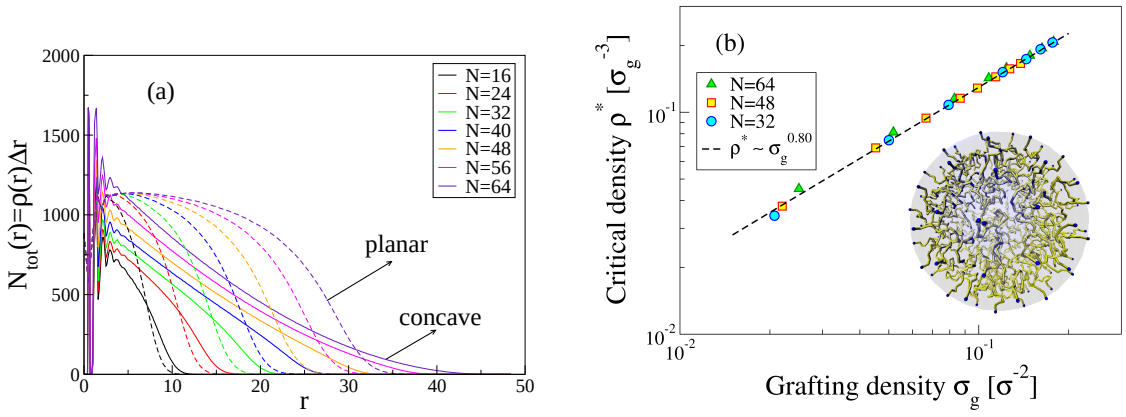

Figure 5: (a) Number of monomers $N_{tot}(r)$ in a spherical segment $r + \Delta r$ at distnave $R - r$ from the spherical shell against the same at distance r from a planar brush for several chain lengths N as indicated. Here the cavity radius $R = 48.5$ and the grafting density $\sigma_g = 0.11$. (b) The same for the total monomer density ρ^* in spherical cavities with critical radius R^*. The snapshot displays a concave brush with $\sigma_g = 0.029$, $N = 32$ at $R^* = 20.1$ where the anchoring beads are shown in blue.

one. In Fig.5b we also demonstrate a new finding, namely, that the scaling of the total monomer density, ρ^*, with varying grafting density, σ_g^*, for concave brushes in spherical shells with *critical* radius R^* goes as $\rho^* \propto (\sigma_g^*)^{\delta}$, where the exponent $\delta \approx 0.80$.

3.2 Effect of chain stiffness

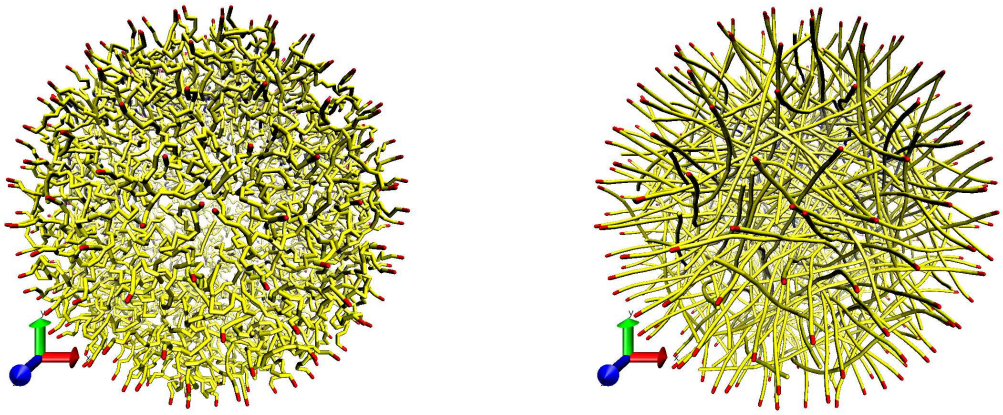

Figure 6: Inwardly grafted brush with chains of length $N = 32$ in a spherical shell with radius $R = 25.5$ at grafting density $\sigma_g = 0.029$ comprised of flexible, $\kappa = 0$, chains (a), and semi-stiff chains, $\kappa = 128$, (b). For better visibility the spherical shell is not shown while the grafting beads are depicted in red.

While in the previous section we have tested SCFT results[31] that concern the behavior of an inwardly bent brush comprised of entirely flexible polymer chains, Fig.6a, it is of interest to see the impact of chain stiffness κ on the properties of concave brushes too. Indeed, one would expect that the structure of a semiflexible polymer brush enclosed in a spherical capsule may change dramatically with growing chain rigidity, e.g., as a consequence of reduced electrostatic screening (salinity) or temperature drop in the solution. In the present study we consider thus sufficiently stiff chains with $\kappa = 128$ whereby the persistence length exceeds considerably their contour length, $\ell_p/(N\sigma) = 4$, Fig.6b.

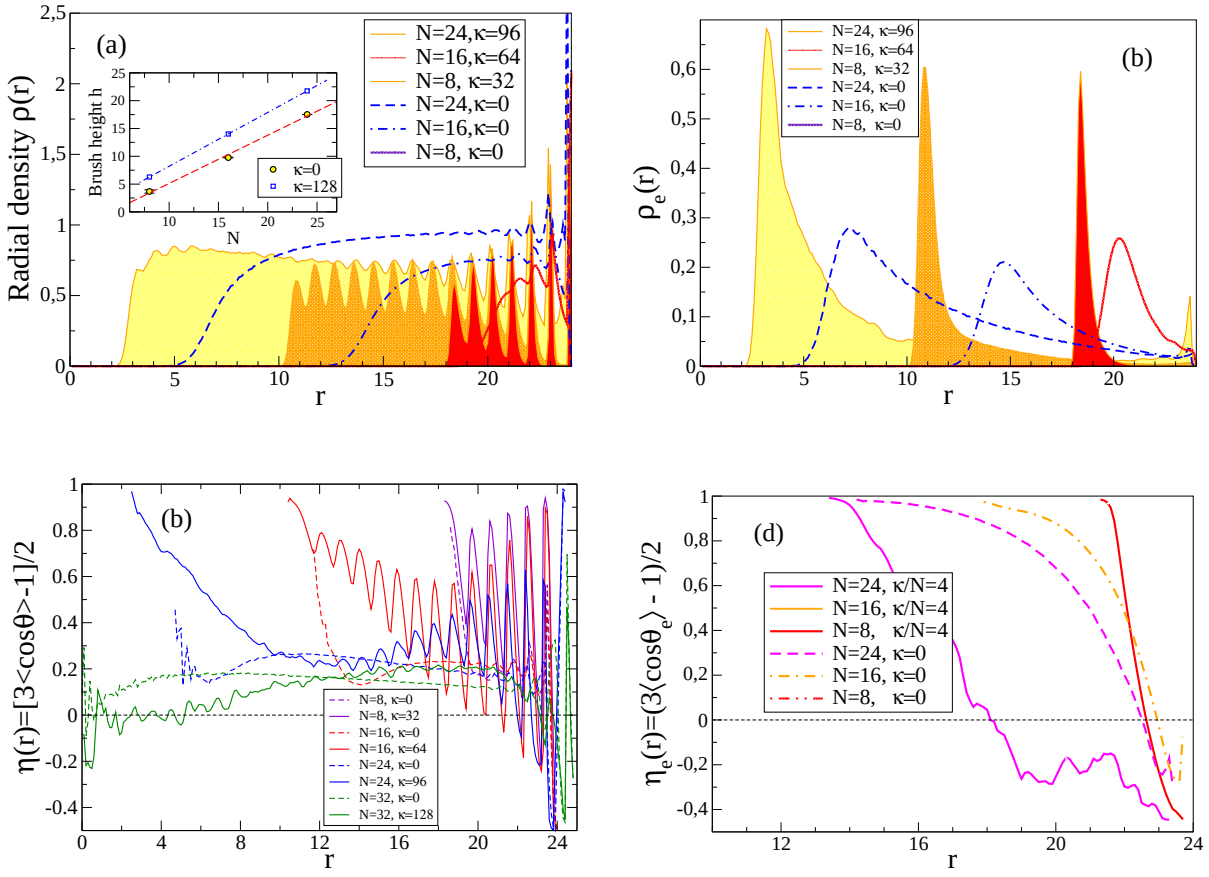

Figure 7: Radial density of monomers, (a), and chain ends, (b), distribution $\rho(r)$ in a shell with radius $R = 24.5$ for a brush at grafting density $\sigma_g = 0.17$ and three molecular weights $N = 8,\ 16,\ 24$. Flexible chains, $\kappa = 0$, (dashed lines), semi-stiff chains with $\ell_p/Nl_b = 4$ (filled full lines). Radial orientation of bonds (c), and of the chains' end-to-end vectors, (d).

To this end in Fig.7a we compare the radial density profiles of inwardly grafted soft ($\kappa = 0$) and stiff ($\ell_p/Nl_b = 4$) brushes with length $8 \leq N \leq 24$ in a spherical shell with radius $R = 24.5$ at a constant grafting density $\sigma_g = 0.17$. Evidently, one observes here qualitatively different density profiles, $\rho(r)$, whereby the usual gradual S-like tail of the brush radial density distribution is replaced by an abrupt end in the case of increased rigidity. As indicated in the inset of Fig.7a, however, the height $h(r)$ scales linearly with chain length N as expected for the regime 2, cf. Fig.1c, of weak concave brushes. The distributions of chain ends, Fig.7b, clearly support the conclusions above. In Fig.7c one can verify that the bonds in the stiff concave brushes are much more strongly oriented along the radial direction than in the flexible brushes. Close to the grafting surface as well as for shorter chains $\eta(r)$ displays typical oscillations in the consecutive bonds orientation. Also the orientation of the end-to-end vectors of the polymer chains, Fig.7d, differs markedly when a stiff concave brush is compared with a flexible one.

As the stiff concave brushes reach much further inwards to the cavity center, one may also expect that for longer chains the distribution of local pressure along and perpendicular to the grafting spherical shell will also reveal significant differences, as demonstrated in the next section.

3.3 Pressure profiles

To find the normal, $P_N(r)$, and transverse, $P_T(r)$, components of the pressure tensor as a function of radial distance r from the center of the cavity, we follow the coarse graining procedure suggested by Nakamura et al.[41] for a spherical geometry, whereby the pressure components at r, cf. Eqs.(5), (6), are calculated as averages over thin spherical layers of finite thickness so as to improve statistics and avoid divergences in $P_T(r)$.

In Fig.8 we show first results for the change of the radial pressure profiles, $P_N(r)$ and $P_T(r)$, of an inwardly curved brush comprised of polymer chains with molecular weight $N = 32$ in a shell of radius $R = 25.5$ for gradually increasing grafting density σ_g. In the

case of flexible chains, $\kappa = 0$, one can see that depending on the degree of cavity filling both $P_N(r)$ and $P_T(r)$ gradually change sign

and grow as the repulsive outer shell is approached. Thus the local pressure P_N at the center of the capsule is nearly zero and attains a maximum in the vicinity of the spherical wall. In contrast, for the stiff chains, $\kappa = 128$, the picture is qualitatively different. Not only is $P_N(r)$ several times stronger than in the respective case of a soft brush but for sufficiently filled cavity, $\sigma_g > 0.10$, one observes a gradual decline in both $P_N(r)$ and $P_T(r)$ as one moves outwards from the center. In fact, the course of $P_N(r)$ and $P_T(r)$ is understandable, given the respective density profiles $\rho(r)$, shown in Fig.8 g, h. Qualitatively, the picture resembles the force profile exerted by an encapsulated *convex* spherical polymer brush on an enclosing cavity wall[29]. One can compare the normal pressure of the brush exerted on the surrounding spherical shell for different chain stiffness, Fig.9a, which is found to scale rather well with the grafting density as $P_N(R) \propto \sigma_g^{4.1\pm0.1}$ regardless of the brush stiffness. Here the pressure exerted by the rigid brush exceeds that of the soft one by a factor of two, $P_N(\kappa = 128)/P_N(\kappa = 0) \approx 2.0$, for the chosen system. One should note, however, that $P_N(R)$ varies here in a rather narrow interval of σ_g so that the scaling exponent could not be determined with sufficient accuracy.

Using the radial profiles of the normal, $P_N(r)$, and tangential, $P_T(r)$, pressure as well as Eq.(7) for γ, we derive the variation of the surface tension γ

in the case of a flexible and stiff concave brush as function of the grafting density, Fig.9. While for a soft concave brush γ stays negative and grows in absolute value steadily with increasing σ_g, in the the case of a stiff polymer brush one observes a nonmonotonic change of γ which becomes negative for $\sigma_g \geq 0.08$ exceeding $\gamma(\kappa = 0)$ for $\sigma_g = 0,17$ by more than a factor of two.

It should be emphasized here that the observed behavior of the surface tension γ with

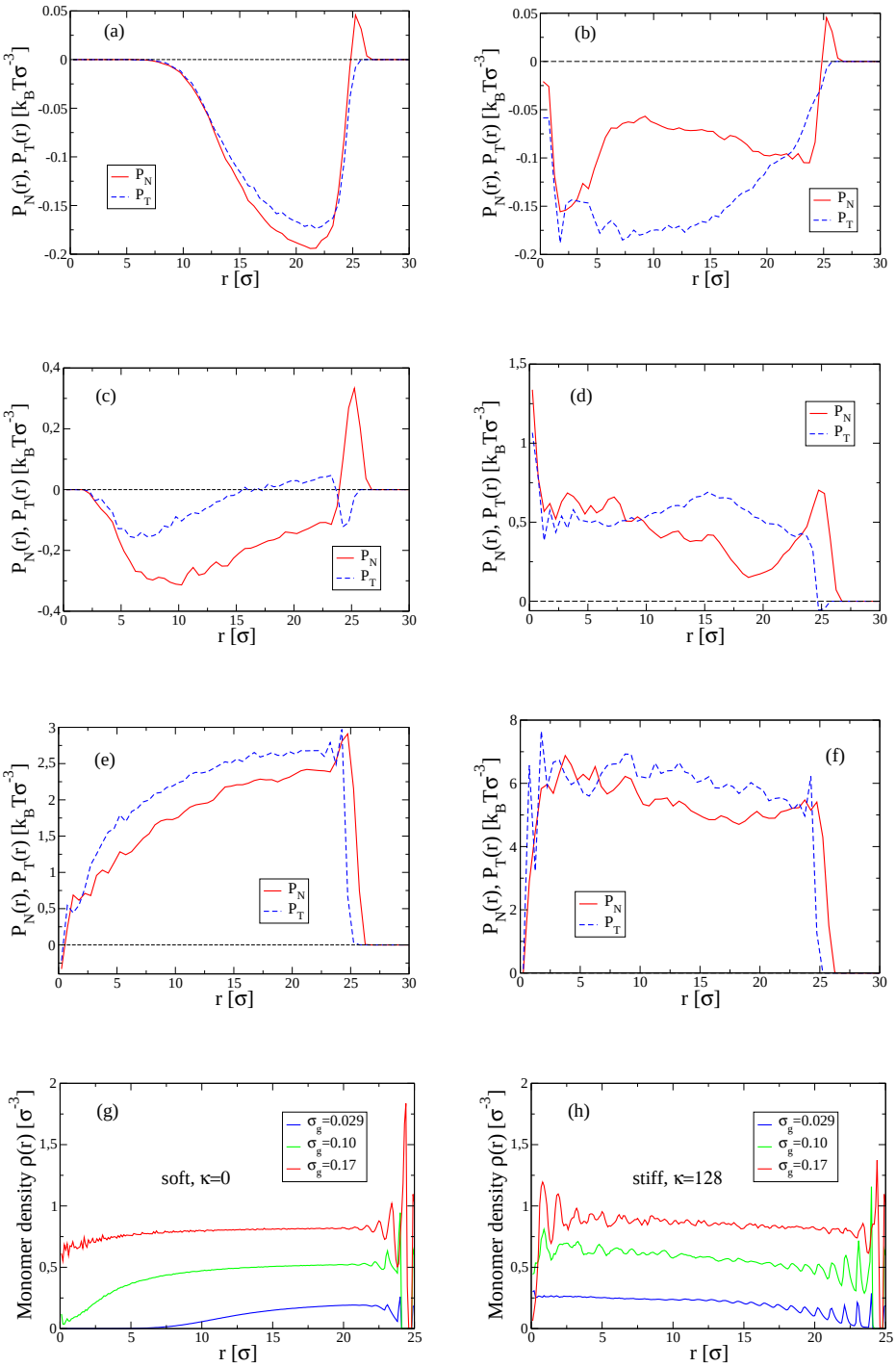

Figure 8: Radial pressure profiles of the normal, $P_N(r)$, and tangential, $P_T(r)$, components of the virial for a polymer brush with chain length $N = 32$ in a spherical cavity of radius $R = 25.5$ for grafting density $\sigma_g = 0.029$ (a, b), $\sigma_g = 0.10$ (c,d), and $\sigma_g = 0.17$ (e, e). The chain stiffness is $\kappa = 0$ (left column), and $\kappa = 128$ (right column). The respective density profiles $\rho(r)$ for flexible and rigid chains are shown in (g) and (h).

Accepted to J. Chem. Phys. 10.1063/5.0141450

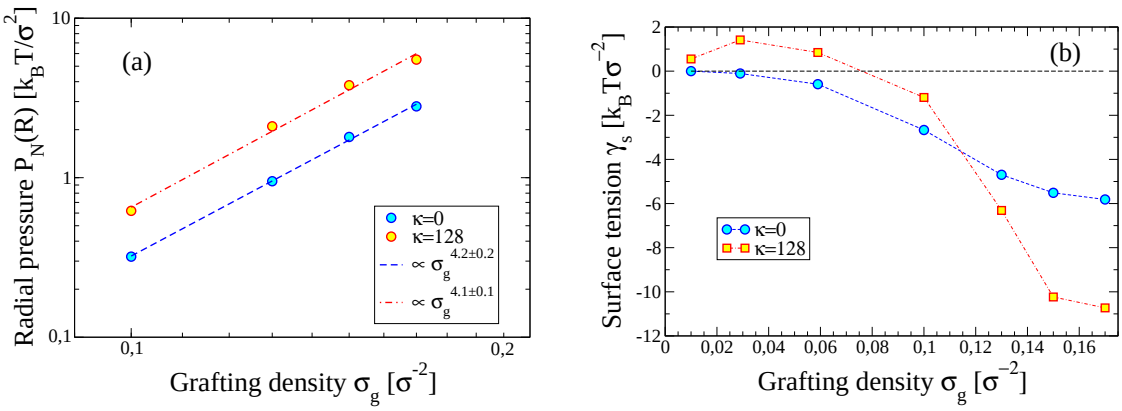

Figure 9: (a) Scaling of the normal pressure exerted on the spherical shell with varying grafting density σ_g. (b) Variation of the surface tension γ with changing grafting density σ_g of an inwardly grafted polymer brush comprised of chains with $N = 32$ in a spherical shell with $R = 25.5$.

varying grafting density σ_g is itself an unique effect characteristic for concave brushes. Indeed, a close inspection of Fig.8a-f and Fig.9b suggests that the sign and the observed variation of γ with σ_g result unambiguously from both the grafting of the polymer chains and the impact of curvature on the radial distribution of monomers within the sphere. Moreover, we have checked that if the tethers to the surface shell are cut, increasing thus the entropy of the confined polymer chains, the surface tension γ becomes positive.

So, for *flexible* chains and contour length of the chains $L \leq R^*$, the empty core of the confining sphere gives rise entropically to a force that *pulls* on the anchoring monomer towards the sphere center, i.e., $P_N(r) < 0$ and $P_T(r) < 0$ while $P_T > P_N$. In contrast, for $L > R^*$, that is, for $\sigma_g = 0.17$, cf. Fig.8e, the sphere center is densely filled and the forces along the chain *press outwards* on the anchoring bead, similar to a compressed spring with both ends fixed, while $P_T > P_N$ again. Apparently, for flexible grafted chains the radial component of the forces is always weaker than the tangential one so that $\gamma < 0$ according to Eq.(7). For *semi-flexible* chains grafted to a concave surface, however, chain rigidity in combination with surface curvature impose preferentially a radial orientation of the chains thereby enhancing the radial repulsion at the expense of the tangential one. In a nearly empty shell, Fig.8b, $P_N > P_T$ in the interior as the chains hardly touch each other laterally

due to their somewhat rodlike conformations. Therefore, for small σ_g one finds $\gamma > 0$. In a semi-filled shell, $\sigma_g > 0.10$, Fig.8d, f, the rigid chains have already both their ends fixed at the origin and at the surface which makes them buckle laterally, resulting in $P_T > P_N$ and thus in $\gamma < 0$.

Therefore, the negative interfacial tension here is due to the specific conformation of the inwardly bent concave polymer brush, yet negative values of γ have been found before also for non-ionic PEG surfactant $C_{12}E_8$ micelles[41] and sodium dodecyl sulfate (SDS) micelles[46], stabilizing such micelles in water.

Summary

In the present work we have studied the structure and scaling behavior of concave polymer brushes inwardly grafted to a spherical surface under good solvent conditions and changing chain length, stiffness, and grafting density of the brush. In the case of flexible chains we have found the critical radius of the cavity, R^*, separating the region of weak curvature in the phase diagram[31], from that of compressed brush.

In the regime of small curvature, $R > R^*$, the brush height $h(N)$, Fig.2b, deviates quadratically from the linear relationship, $h_{plan} \propto N$, as predicted[31]. Just as in planar brushes, we also find in this regime $h \propto \sigma_g^{1/3}$, see Fig.3b, whereas the variation of R^* with σ_g yields a scaling exponent $R^* \propto \sigma_g^{\alpha}$ with $\alpha \approx 0.23$ which is less than the asymptotic value $\alpha = 1/3$, predicted by SCFT[31] due to finite-size effects, since $N \leq 64$, $R \leq 48.5$, of the systems studied. In agreement with theoretical predictions, the density distribution of chain ends, $\rho_e(r)$, develops a sharp maximum with growing $R^*(\sigma_g)$ which is found to approach asymptotically the cavity center as $r^e_{max} \propto (\sigma^*_g)^{-0.56}$. A scaling relationship is also found which describes the variation of the critical density, ρ^*, of a capsule with critical radius R^* resulting from the corresponding grafting density, $\rho^* \propto \sigma_g^{0.80}$.

While the aforementioned results concern flexible concave brushes, in the second section

of our results we have demonstrated the impact of chain stiffness on the properties of inwardly bent polymer brushes in a capsule. One may verify from Fig.6 that the density distributions of monomers and chain ends as well as the radial orientaion of bonds and end-to-end vectors of chains change qualitatively.

Finally, we obtain the radial profiles of normal, $P_N(r)$, and transverse, $P_T(r)$, local pressure of a concave brush in a spherical capsule, Fig.8, for both flexible and semiflexible polymer chains which can be assessed in conjunction with the corresponding density profiles, $\rho(r)$. Interestingly, it is found that the normal pressure exerted on the spherical shell of radius R scales as $P_N(R) \propto \sigma_g^4$ irrespective of the particular chains stiffness even though $P_N(R)$ for stiff chains with $\ell_p/(Nl_b) = 4$ is about twice stronger than for soft chains. In contrast, our data reveal a qualitative contrast in the surface tension γ variation with grafting density σ_g.

We believe that this study provides new insights into the properties of inwardly bent concave polymer brushes in spherical capsules which might initate further investigations and serve as ground for possible applications.

Acknowledgments

A.M. thanks the COST action No. CA17139, supported by COST (European Cooperation in Science and Technology). A. M. acknowledges DFG support under Project No. NI 1487/2-2.

References

(1) Chen, W. L., Cordero, R., Tran, H., Ober, C. K., *50th Anniversary Perspective: Polymer Brushes: Novel Surfaces for Future Materials*, Macromolecules **50**, 4089 - 4113 (2017).

(2) Ankit Shukla, A., Tiwari, S., Singh, M. P., Singh, S., Singh, M. K., Kumar A., *compre-*

hensive review on polymeric micelles: a promising drug delivery carrier J. Anal. Pharm. Res. **10**, 102 725

(3) Dubashynskaya, N., Poshina D., Raik, S., Urtti, A., Skorik, Y. A., *Polysaccharides in Ocular Drug Delivery*, Pharmaceutics, **12**, 22 (2020).

(4) *Smart Nanoparticles for Drug Delivery Application: Development of Versatile Nanocarrier Platforms in Biotechnology and Nanomedicine*, Lombardo, D., Kiselev, M. A., Caccamo, M. T., J. of Nanomaterials, **2019**, Article ID 3702518 (2019)

(5) *Heterogeneous Synthetic Vesicles toward Articial Cells: Engineering Structure and Composition of Membranes for Multimodal Functionalities*, Shin, J., Cole, B. D., Shan, T., Jang, Y., Biomacromolecules, **23** 1505 - 1518(2022).

(6) , *Stimuli-responsive polymer brushes for flow control through nanopores*, Adiga, S., Brenner, D. W., J. Funct. Biomater. , **3**, 239-256 (2012).

(7) Chen, G., Das, S. *Electroosmotic transpoet in polyelectrolyte-grafted naanochannels with pH-dependent charge density*, J. Appl. Phys. **117**, 185304 (2015).

(8) Luzinov, I., Minko, S., Tsukruk, V. V., *Responsive brush layers: from tailored gradients to reversibly assembled nanoparticles*, Soft Matter, **4**, 714 - 725 (2008). 714–725

(9) *Functional polymer brushes in aqueous media from self-assembled and surface-initiated polymers*, Toomey, R., Tirrell, M., Annual Rev. Phys. Chem. **59**, 493 - 517 (2008).

(10) P. G. de Gennes *Scaling Concepts in Polymer Physics*, Cornell University Press, Ithaca, 1979.

(11) Alexander, S., *Adsorption of chain molecules with a polar head a scaling description*, J. Physique, **38**, 983 - 987 (1977).

(12) Dimitrov, D., Milchev, A., Binder, K., *Polymer brushes in solvents of variable quality: molecular dynamics simulations using explicit solvent*, J. Chem. Phys. **127**, 084905 (2007).

(13) Suk, J. S., Xu, Q., Kim, N., Hanes, J., Ensign, L. M., *PEGylation as a strategy for improving nanoparticles-based drug and gene delivery*, Adv. Drug Deliv. Rev. **99**, 28 - 51 (2016).

(14) Shamsi Jazeyi, H., Miller, C. A., Wong, M. S., Tour, J. M., Verduzco, R., *Polymer-coated nanoparticles for enhanced oil recovery*, J. Appl. Polym. Sci. **131**, 40576 (2014).

(15) Zoppe, J. O., Venditti, R. A., Rojas, O. J., *Pickering emulsions stabilzed by cellulose nanocrystals grafted with thermo-responsive polymer brushes*, J. Colloid Interfaces Sci. **369**, 202 - 209 (2012).

(16) Jiang, C., Zhang, Y., Wang, Q., Wang, T., *Superhydrophobic polyurethane and silica nanoparticles coating with high transparency and fluoroescence*, J. Appl. Polym. Sci., **129**, 2959 - 2965 (2013).

(17) Descas, R., Sommer, J.-U., Blumen, A., *Grafted Polymer Chains Interacting with Substrates: Computer Simulations and Scaling*, Macromol. Theory Simul. **17**,429 256 (2006).

(18) Dimitrov, D. I., Milchev, A., Binder, K., *Polymer brushes on flat and curved substrates: scaling concepts and computer simulations*, Macromol. Symp., **252**, 47 - 57 (2007), WILEY-VCH Verlag GmbH & Co. KGaA, Weinheim.

(19) Daoud, M., Cotton, J. P., *Star shaped polymers: a model for the conformation and its concentration dependence*, J. Physique, **43**, 531 - 538 (1982).

(20) Zhulina, E. B.; Birshtein, T. M.; Borisov, O. V. *Curved polymer and polyelectrolyte*

brushes beyond the Daoud-Cotton model, Eur. Phys. J. E: Soft Matter Biol. Phys. **20**, 243 – 256 (2006).

(21) Li, C.-W., Romeis, D., Koch, M., Merlitz, H., Sommer, J.-U., *Theoretical analysis of the elastic energy contributions to polymer brushes in poor solvent: A refined mean-field theory*, J. Chem. Phys. **157**, 104902 (2022).

(22) Lo Verso, F., Egorov, S., Milchev, A., Binder, K., *Spherical polymer brushes under good solvent conditions: molecular dynamics results compared to density functional theory*, J. Chem. Phys. **133**, 184901 (2010).

(23) Romiszowski, P., Sikorski, A., *The structure of polymer chains in confinement. A Monte Carlo study*, J. Mol. Model. **15**, 681 - 686 (2009).

(24) Milchev, A., Binder, K., Heermann, D. W., Dimitrov, D. I., *Structure of polymer brushes in cylindrical tubes: a molecular dynamics simulation*, Macromol. Theory Simul., **15**, 573 - 583 (2006).

(25) Dimitrov, D. I., Milchev, A., Binder, K., *Polymer brushes in cylindrical pores: simulation versus scaling theory*, J. Chem. Phys. **125** 034905 (2006).

(26) Egorov, S. A., Milchev, A., Klushin, L., Binder, K., *Structural properties of concave cylindrical brushes interacting with free chains*, Soft Matter, **7**, 5669 (2011)

(27) Wang, R., Egorov, S. A., Milchev, A., Binder, K., *Stretching of free chains confined in concave brush-coated nanocylinders*, Soft Matter, **45**, 2580 1555, (2012).

(28) Binder, K., Milchev, A., *Polymer brushes on flat and curved surfaces: how computer simulations can help to test theories and to interpret experiments*, J. Polymer Sci. B: Polymer Physics, **50**, 1515 – 1555, (2012).

(29) Cerda, J., Sintes, T. , Toral, R., *Spherical brushes within spherical cavities: A self-consistent field and Monte Carlo study*, J. Chem. Phys. **131**, 134901 (2009)

(30) Laktionov, M. Y., Zhulina, E., B., Richter, R. P., Borisov, O. V., *Polymer Brush in a Nanopore: Effects of Solvent Strength and Macromolecular Architecture Studied by Self-Consistent Field and Scaling Theory*, Polymers, **13**, 392 (2021).

(31) M. Mangi, M. Aubouy, G. Gay and C. Ligoure, Eur. Phys. J. E **5**, 519-530 (2001).

(32) Prochazka, K., *Monte Carlo study of tethered chains in Spherical Volumes*, J. Phys. Chem. **99**, 14108 - 14116 (1995).

(33) Cheng, P.-L., Berney, V. C., Cohen, R. E., *Distribution of chain ends inside the polybutadiene microspheres of styrene-butadiene diblock copolymers*, Macromolecules, **21**, 3442 - 3446 (1988).

(34) Weeks, J. D., Chandler, D., Anderson, H. C. *Role of repulsive forces in determining the equilibrium structure of simple liquids* J. Chem. Phys. **54**, 5237, (1971).

(35) Kremer, K.; Grest, G. S. *Dynamics of entangled linear polymer melts - a molecular dynamics simulation* J. Chem. Phys. **92**, 5057 (1990).

(36) Milchev, A., Egorov, S. A., Nikoubashman, A., Binder, K. *Conformations and orientational ordering of semiflexible polymers in spherical confinement*, J. Chem. Phys. **146**, 194907 (2017).

(37) Allen, M. P., Tildesley, D. J. *Computer Simulation of Liquids* 2^{nd} ed. Oxford University Press, Oxford 2017.

(38) Semechko A., MATLA, https://github.com/AntonSemechko/S2-Sampling-Toolbox

(39) Andersen, L., Lorenz, C., J. Travesset, A. *General purpose molecular dynamics simulations fully implemented on graphics processing units* Comput. Phys. **227**, 5342, (2008).

(40) Glaser, J., Nguyen, T. D., Anderson, J. A., Liu, P., Spiga, F., Millan, J. A., Morse, D. C., Glotzer, S. C. *Strong scaling of general-purpose molecular dynamics simulations on GPUs* Comp. Phys. Comm. **192;**, 197, (2015).

(41) Nakamura, T., Shinoda, W., Ikeshogi, T. *Novel numerical method for calculating the pressure tensor in spherical coordinates for molecular systems*, J. Chem. Phys. **135**, 094106 (2011).

(42) Lovett, R., Baus, M. *A molecular theory of the Laplace relation and of the local forces in a curved interface*, **106**, 635 (1997).

(43) Ghoufi, A., Malfreyt, P., *Local pressure components and surface tension of spherical interfaces. Thermodynamics versus mechanical definitions. I. A mesoscopic modeling of droplets*, J. Chem. Phys. **135**, 104105 (2011)

(44) Zhulina, Ye.-B. *Conformations of Macromolecules Grafted onto Solid Spherical Surface*, Vysokomol. Soed. **B 25**, 834 - 838 (1983).

(45) Amoskov, V., M.; Pryamitsyn, V., A. *Theory of Monolayers of Non-Gaussian Polymer Chains grafted onto a Surface*, J. Chem. Soc. Faraday Trans. **90**, 889 - 893 (1994).

(46) Kitabata, M., Fujimoto, K., Yoshi, N., Okazaki, S., *A molecular dynamics study of local pressure and surface tensions of SDS micelles and dodecane droplets in water*, J. Chem. Phys. **144**, 224701 (2016)

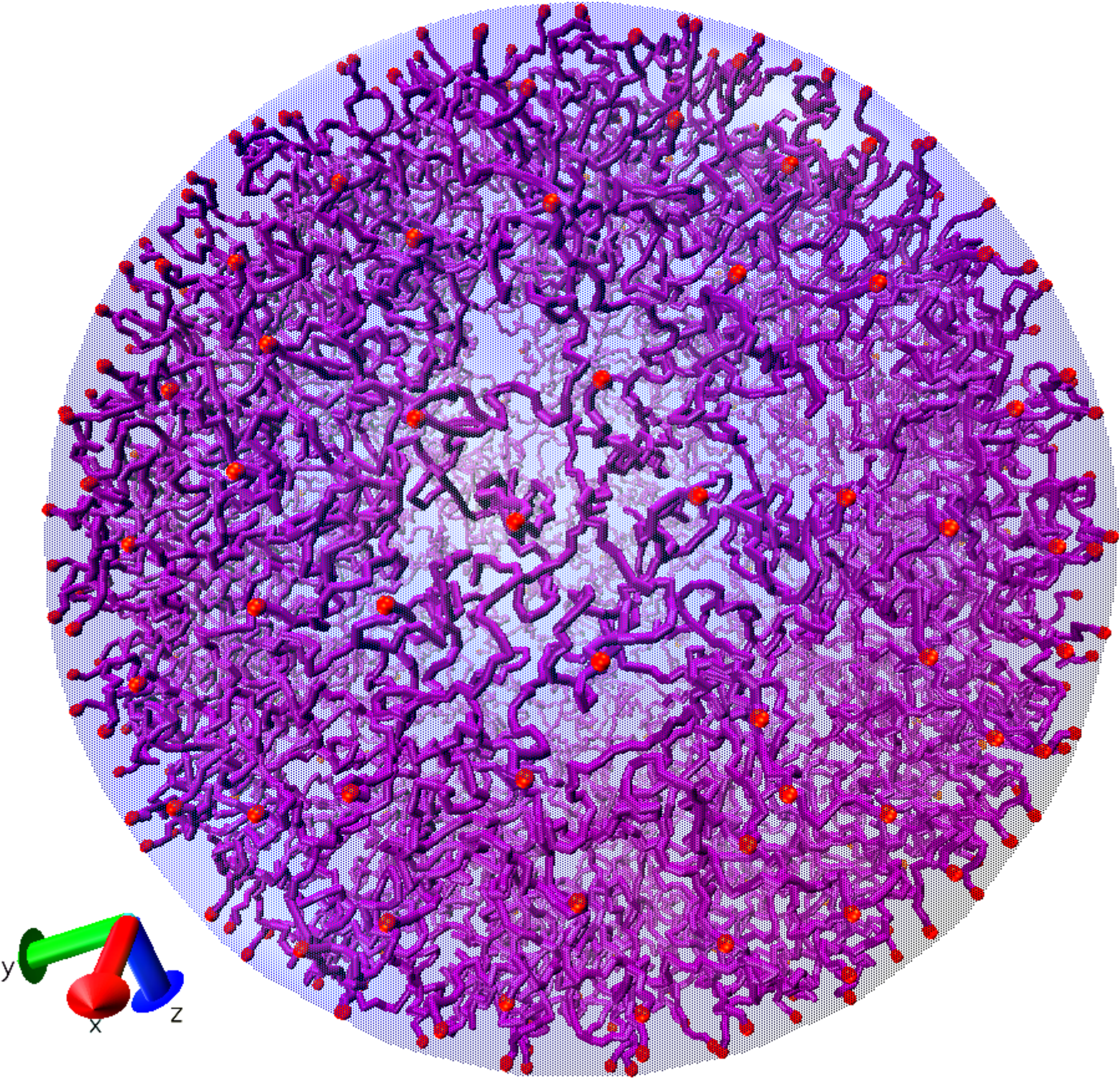
y
x
z

Accepted to J. Chem. Phys. 10.1063/5.0141450

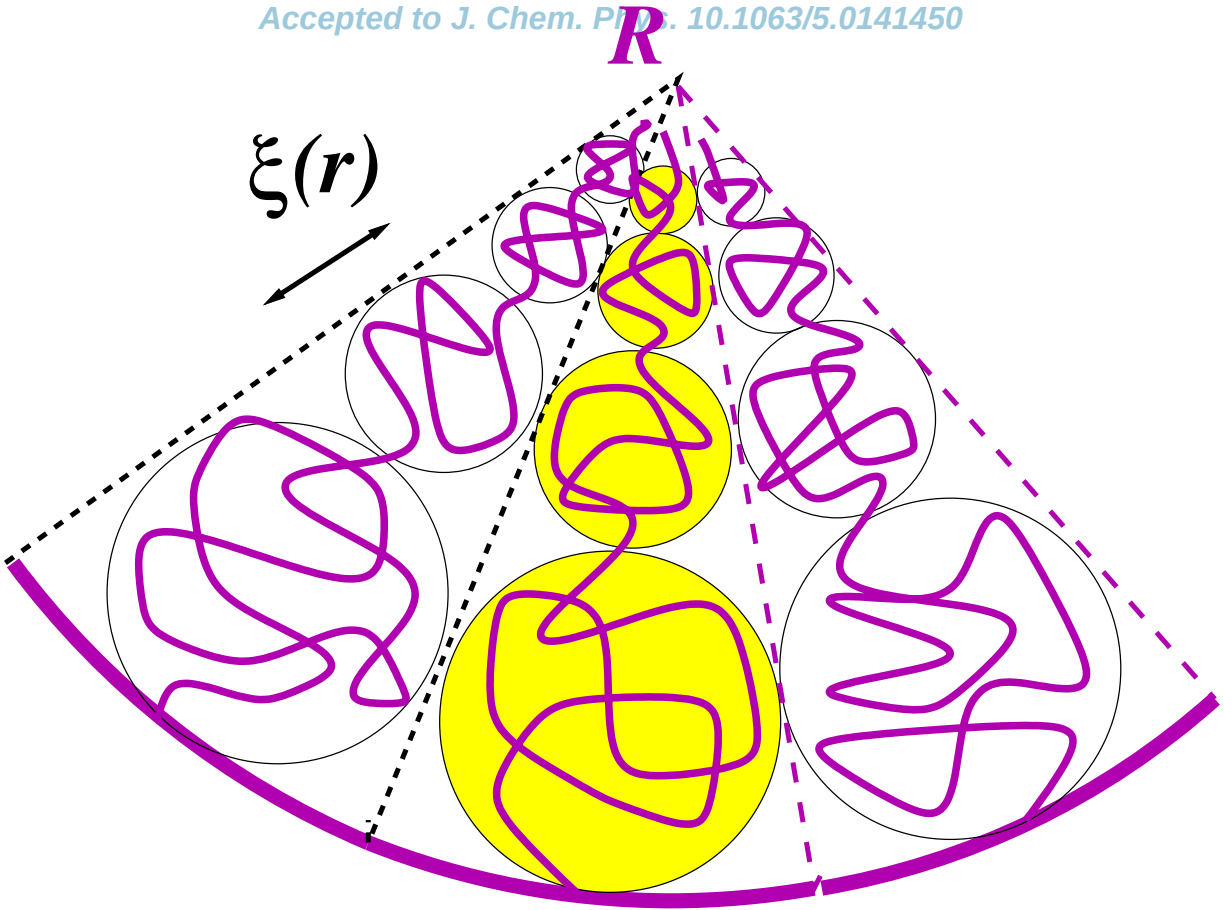

Accepted to J. Chem. Phys. 10.1063/5.0141450

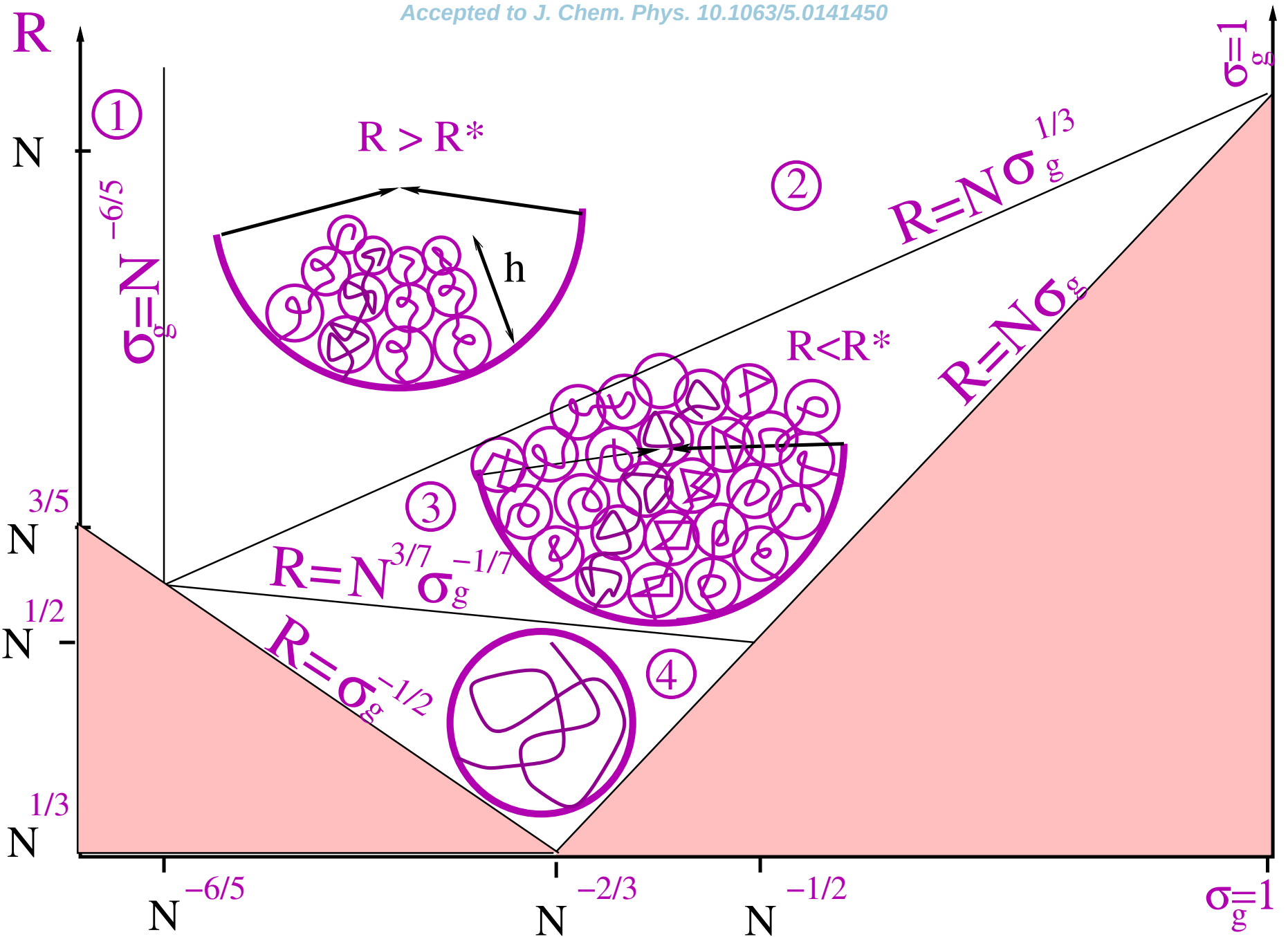

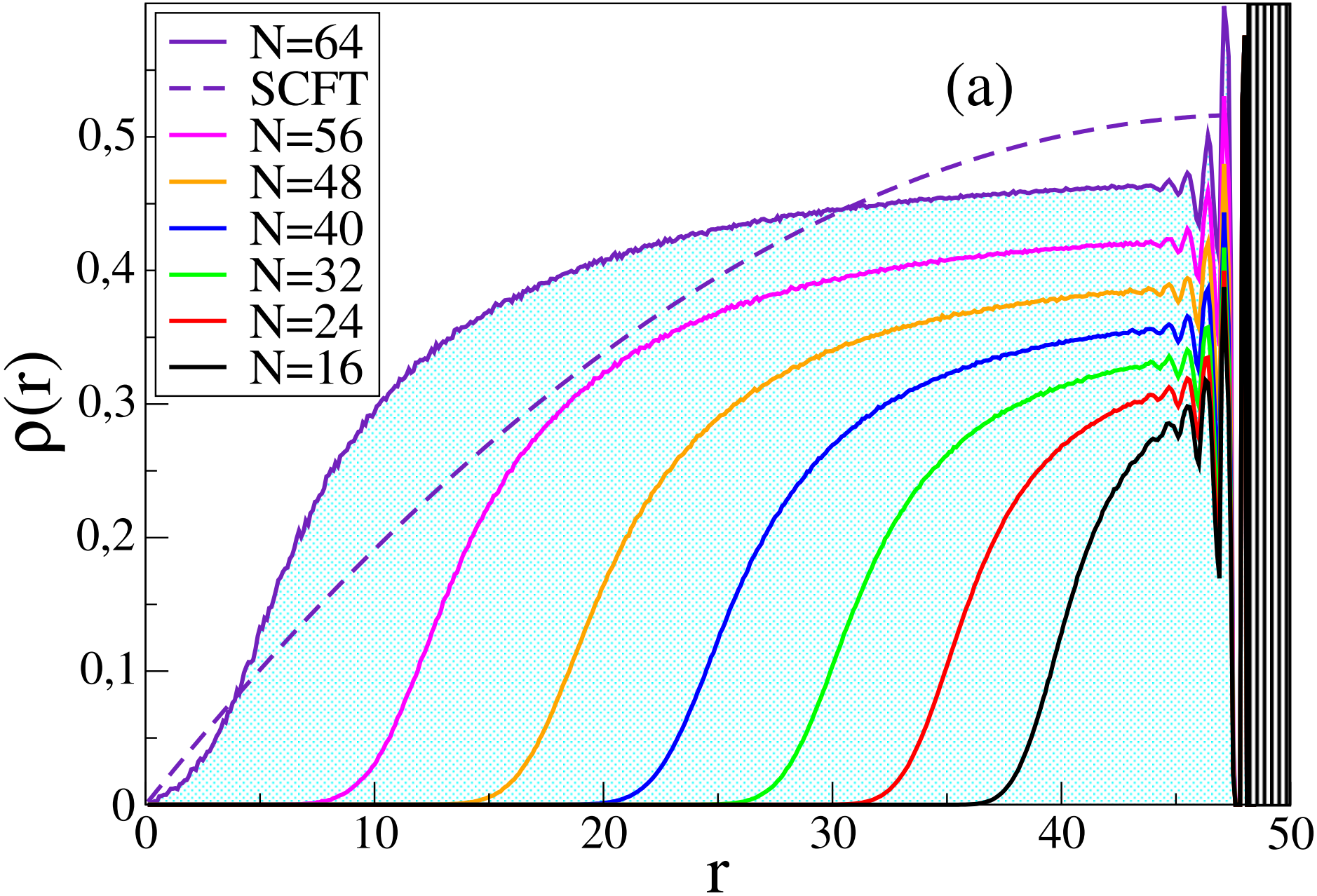
N=64
SCFT
N=56
N=48
N=40
N=32
N=24
N=16
(a)
ρ(r)
r
0
0,1
0,2
0,3
0,4
0,5
0
10
20
30
40
50

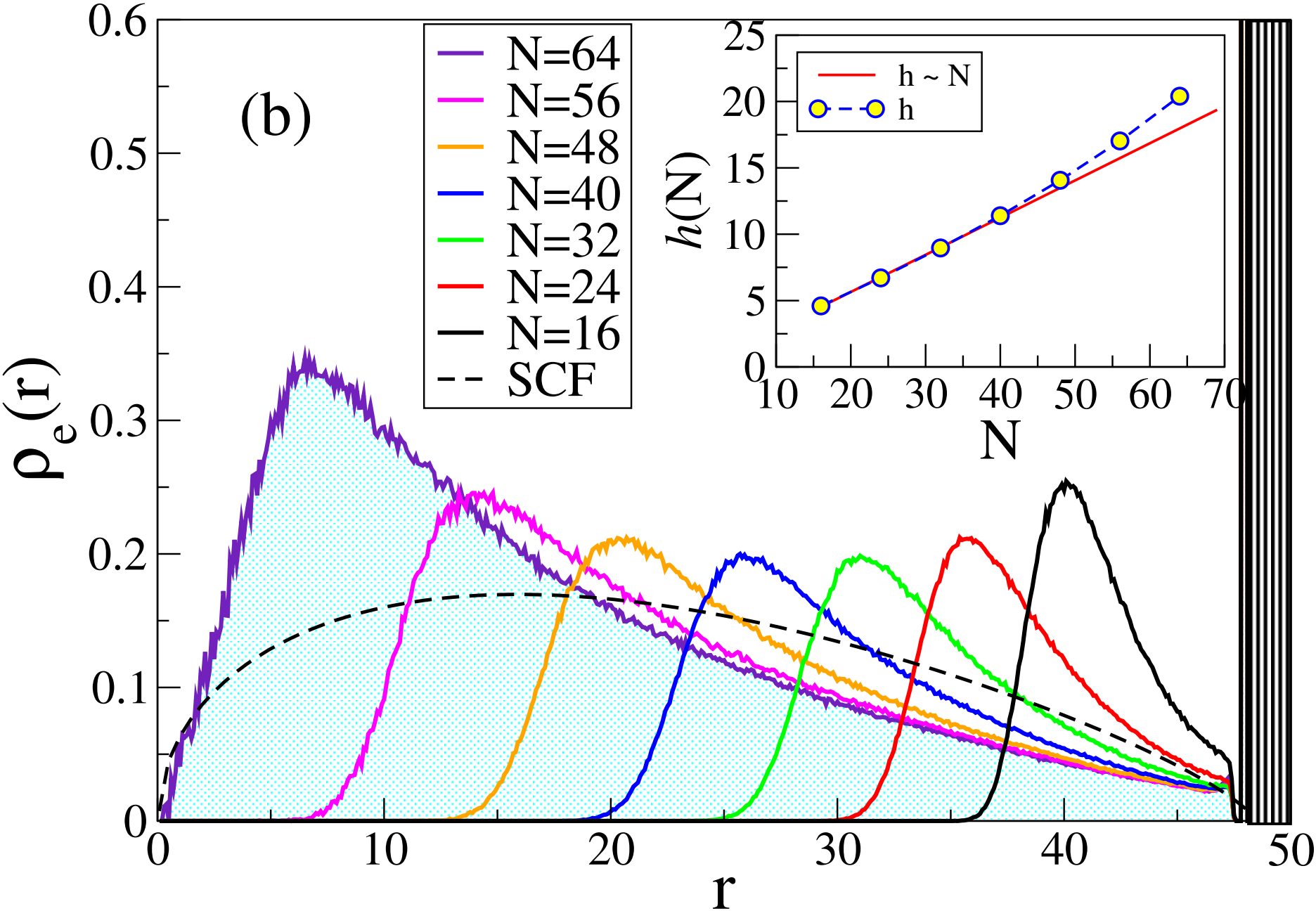
(b)
N=64
N=56
N=48
N=40
N=32
N=24
N=16
SCF
$\rho_e(r)$
r
h ~ N
h
h(N)
N

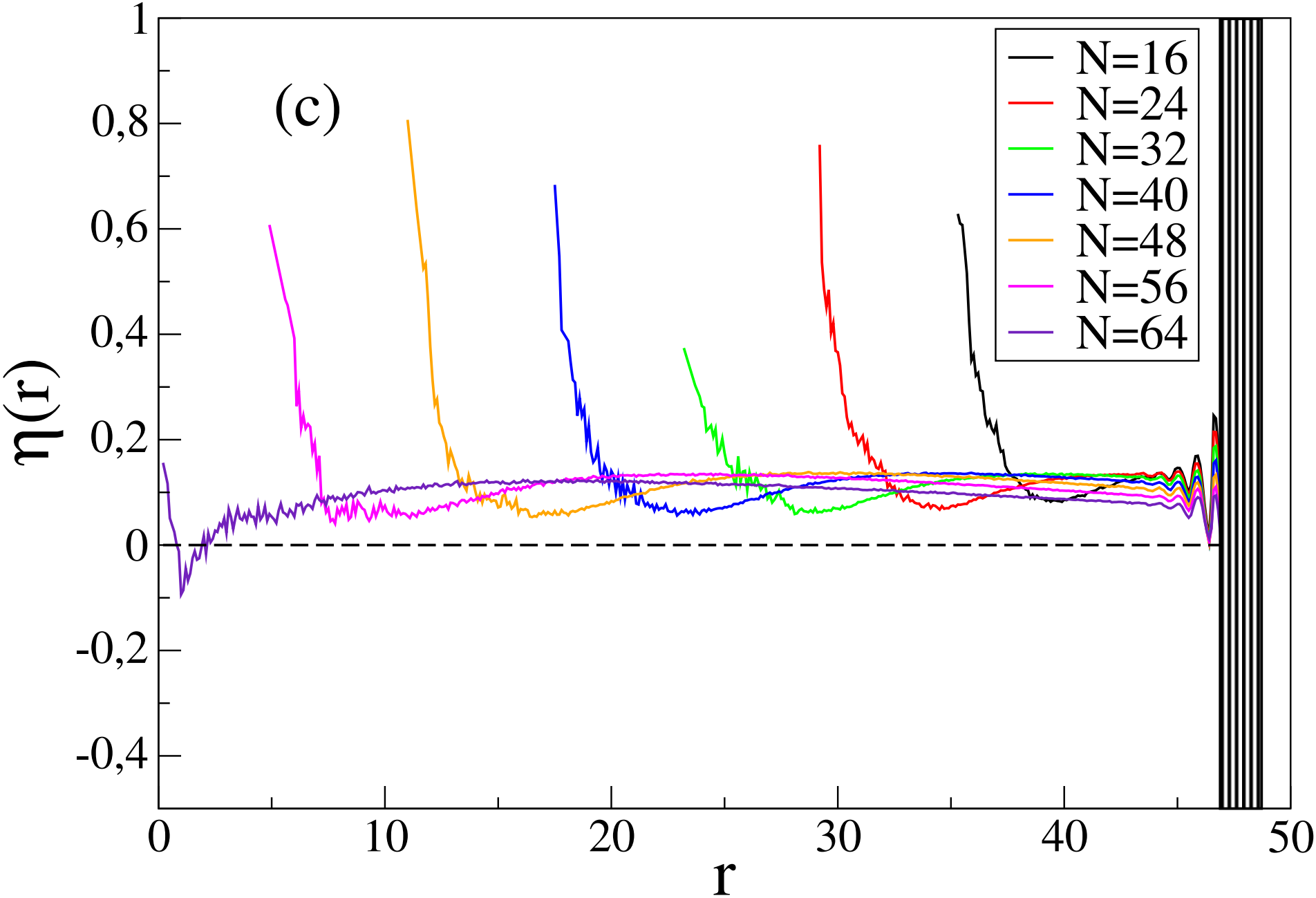
(c)
N=16
N=24
N=32
N=40
N=48
N=56
N=64
η(r)
r
1
0,8
0,6
0,4
0,2
0
-0,2
-0,4
0
10
20
30
40
50

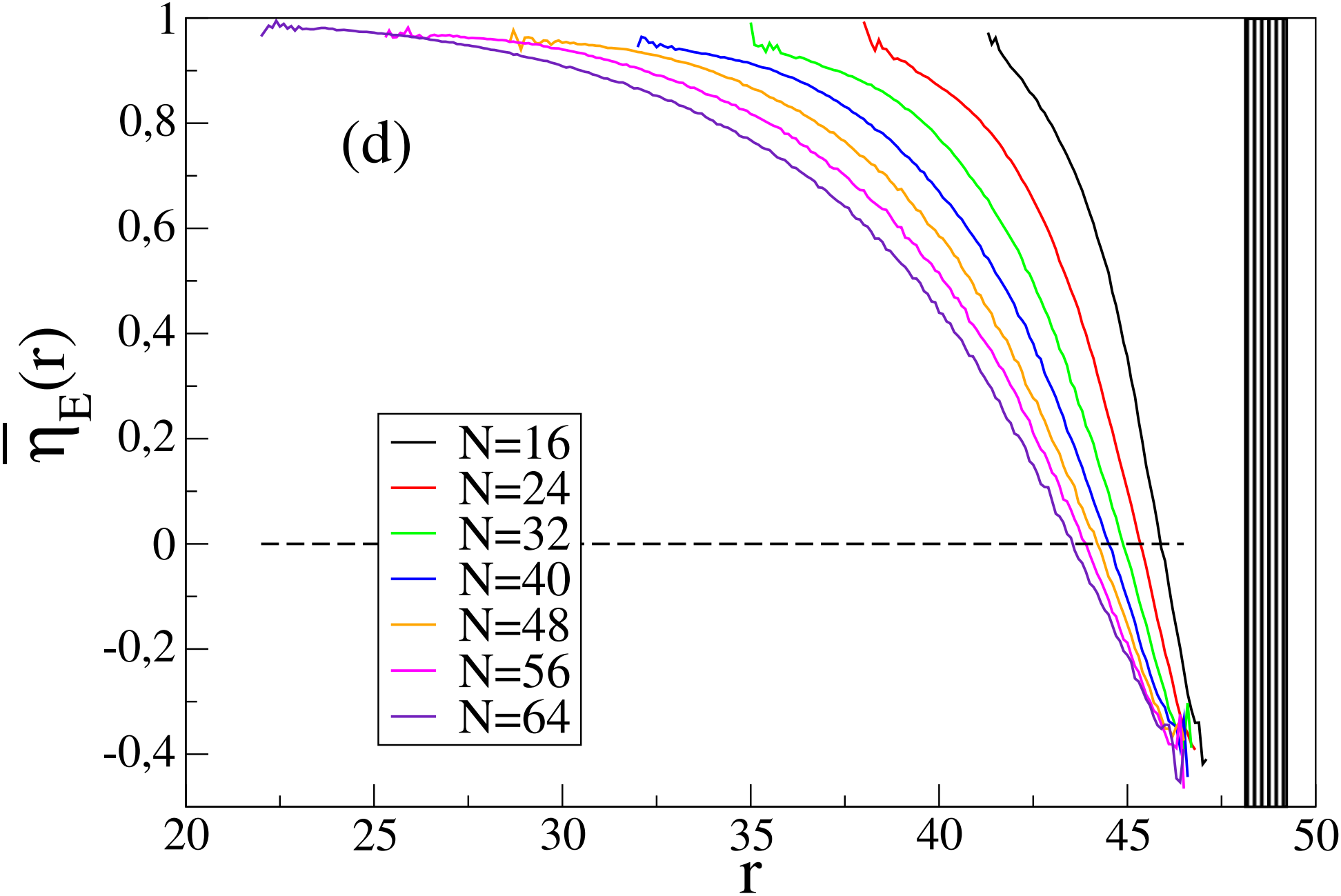
(d)
N=16
N=24
N=32
N=40
N=48
N=56
N=64
$\eta_E(r)$
r
1
0,8
0,6
0,4
0,2
0
-0,2
-0,4
20
25
30
35
40
45
50

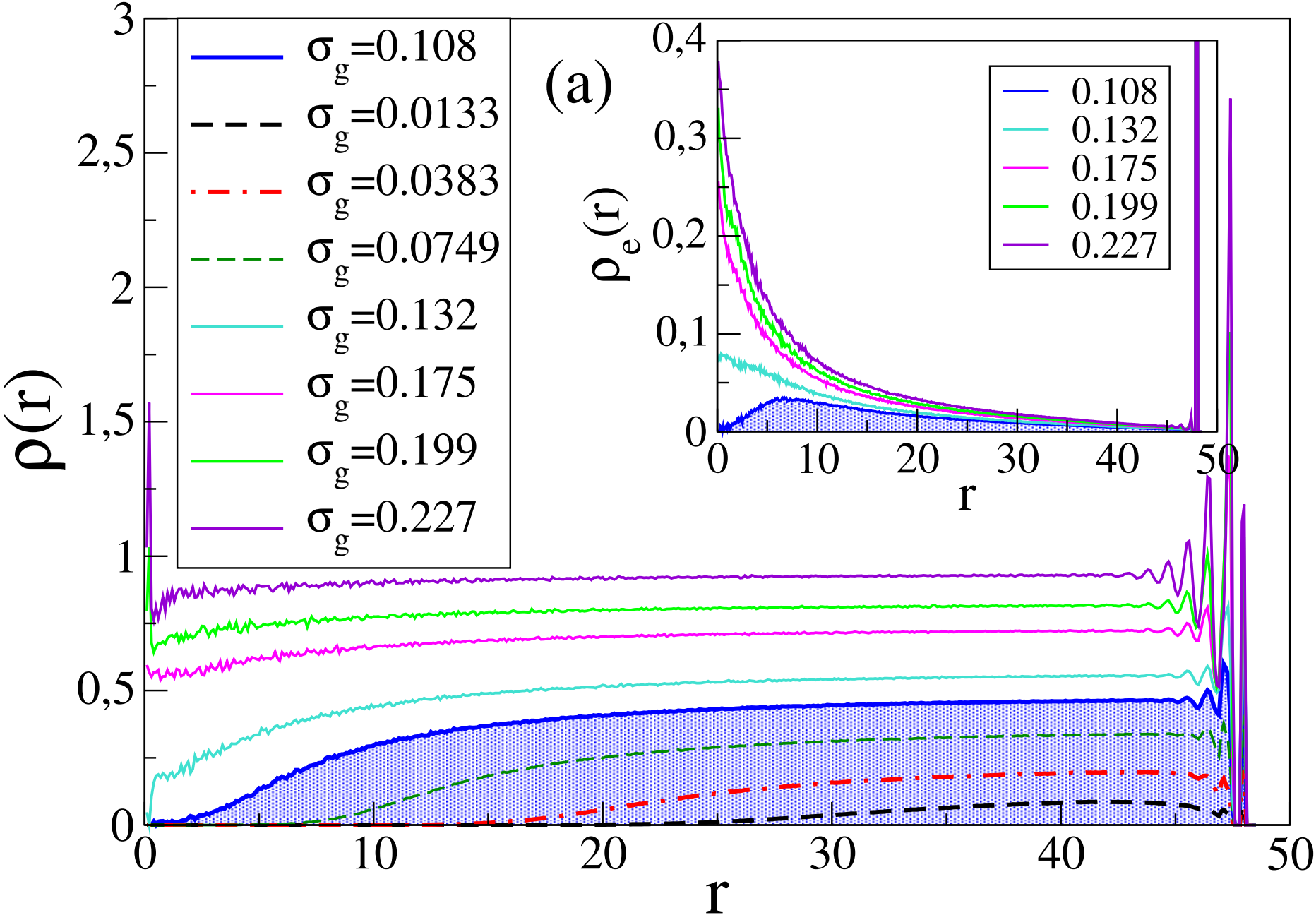
(a)
σg=0.108
σg=0.0133
σg=0.0383
σg=0.0749
σg=0.132
σg=0.175
σg=0.199
σg=0.227
ρ(r)
r
0
0,5
1
1,5
2
2,5
3
0
10
20
30
40
50
ρe(r)
0,1
0,2
0,3
0,4
0.108
0.132
0.175
0.199
0.227

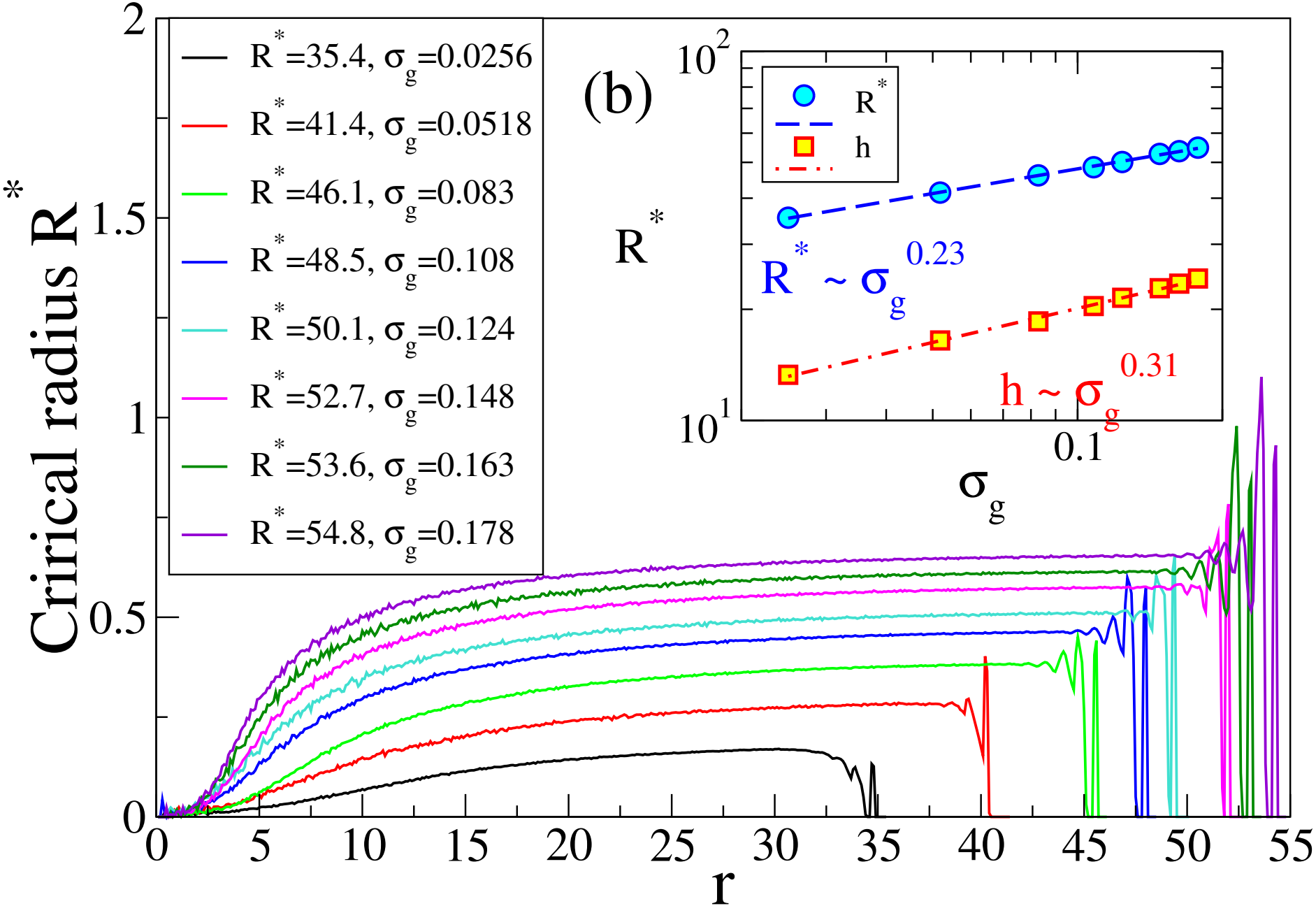
(b)
R* =35.4, σg=0.0256
R* =41.4, σg=0.0518
R* =46.1, σg=0.083
R* =48.5, σg=0.108
R* =50.1, σg=0.124
R* =52.7, σg=0.148
R* =53.6, σg=0.163
R* =54.8, σg=0.178
Cririal radius R*
r
R*
h
R* ~ σg 0.23
h ~ σg 0.31
σg
10^2
10^1
0.1
0
0.5
1
1.5
2
5
10
15
20
25
30
35
40
45
50
55

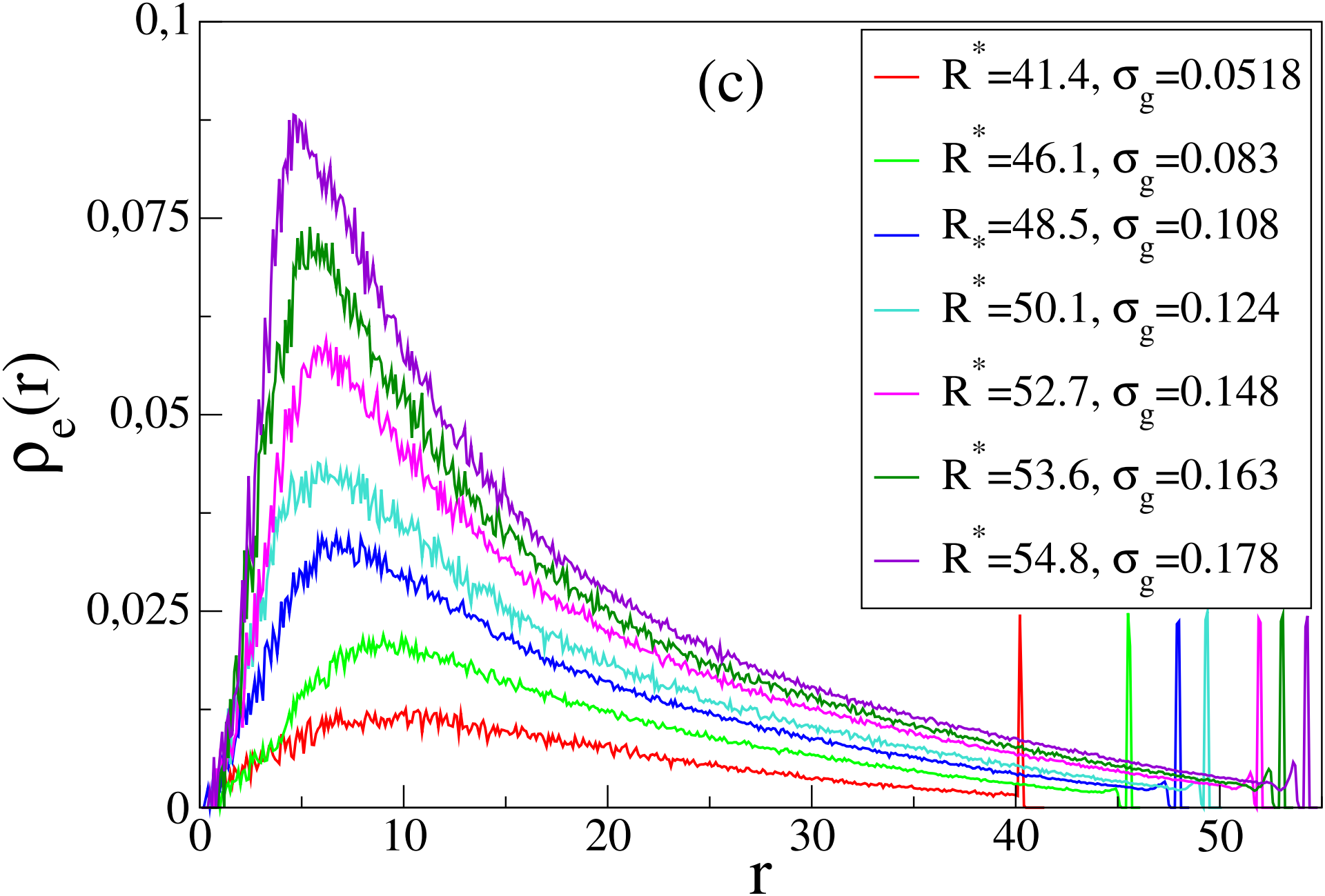
(c)
R*=41.4, σg=0.0518
R*=46.1, σg=0.083
R*=48.5, σg=0.108
R*=50.1, σg=0.124
R*=52.7, σg=0.148
R*=53.6, σg=0.163
R*=54.8, σg=0.178
ρe(r)
r
0,1
0,075
0,05
0,025
0
0
10
20
30
40
50

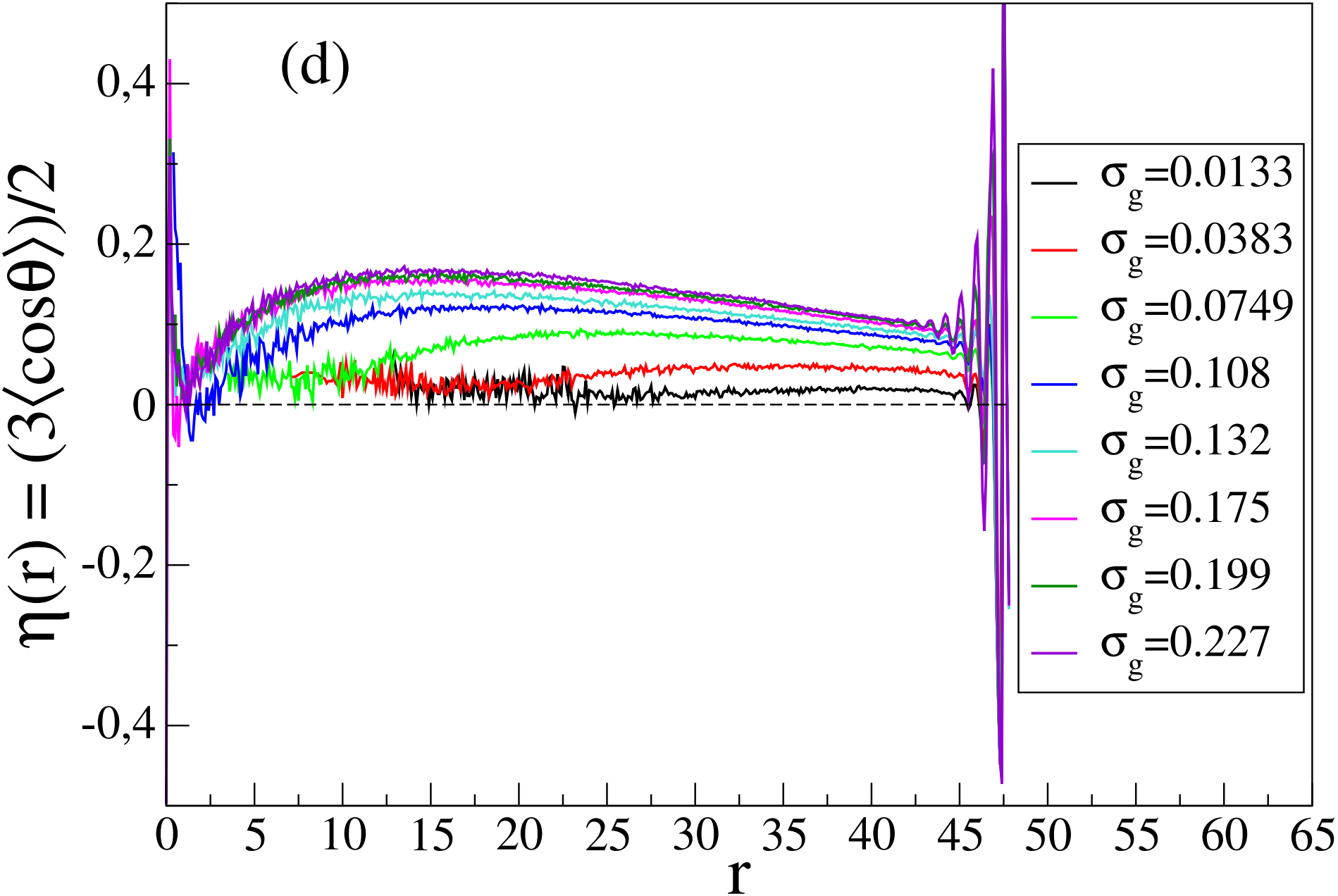
(d)
0,4
0,2
0
-0,2
-0,4
η(r) = (3⟨cosθ⟩)/2
0
5
10
15
20
25
30
35
40
45
50
55
60
65
r
σg=0.0133
σg=0.0383
σg=0.0749
σg=0.108
σg=0.132
σg=0.175
σg=0.199
σg=0.227

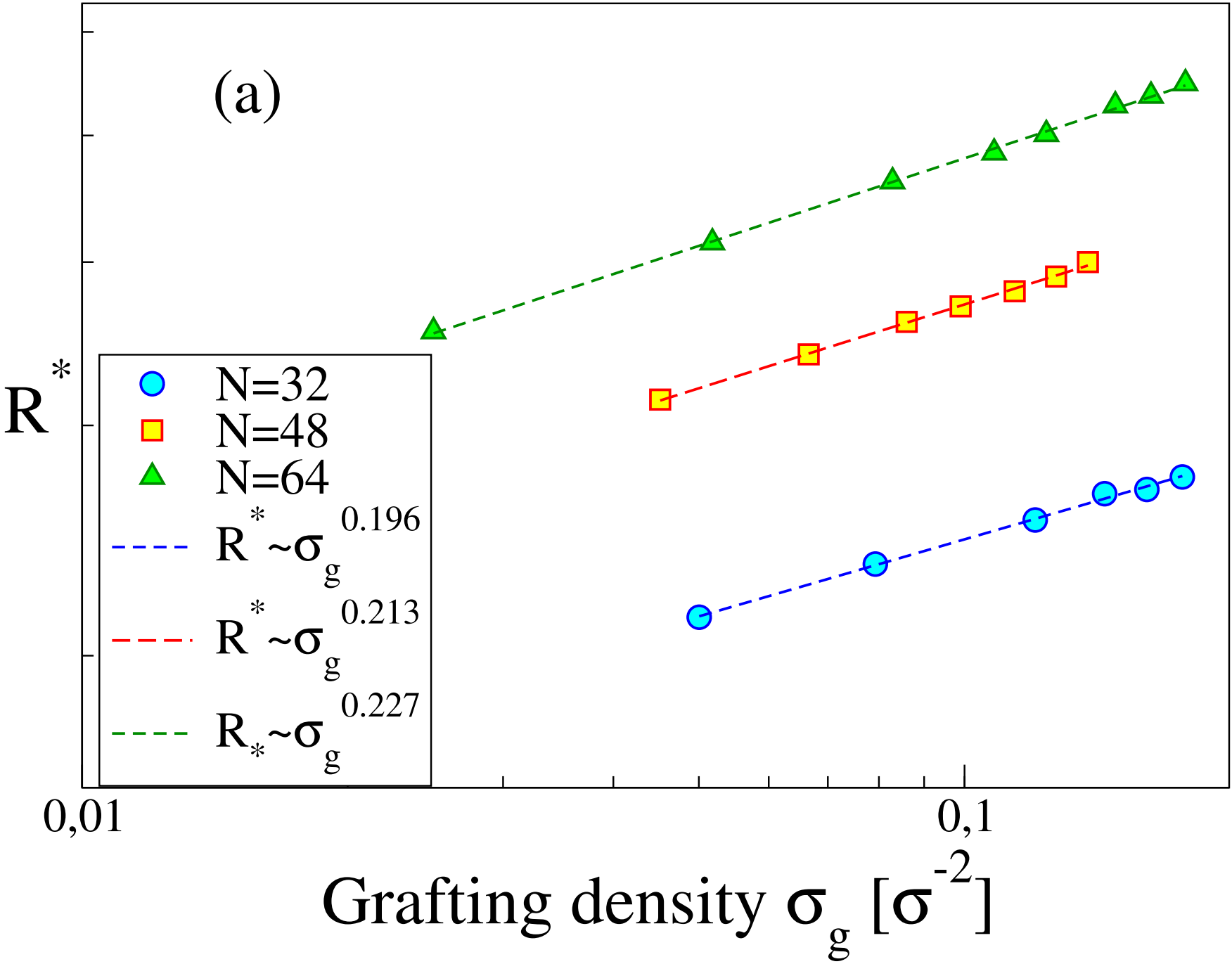
(a)
R*
N=32
N=48
N=64
R* ~σg 0.196
R* ~σg 0.213
R* ~σg 0.227
0,01
0,1
Grafting density σg [σ-2]

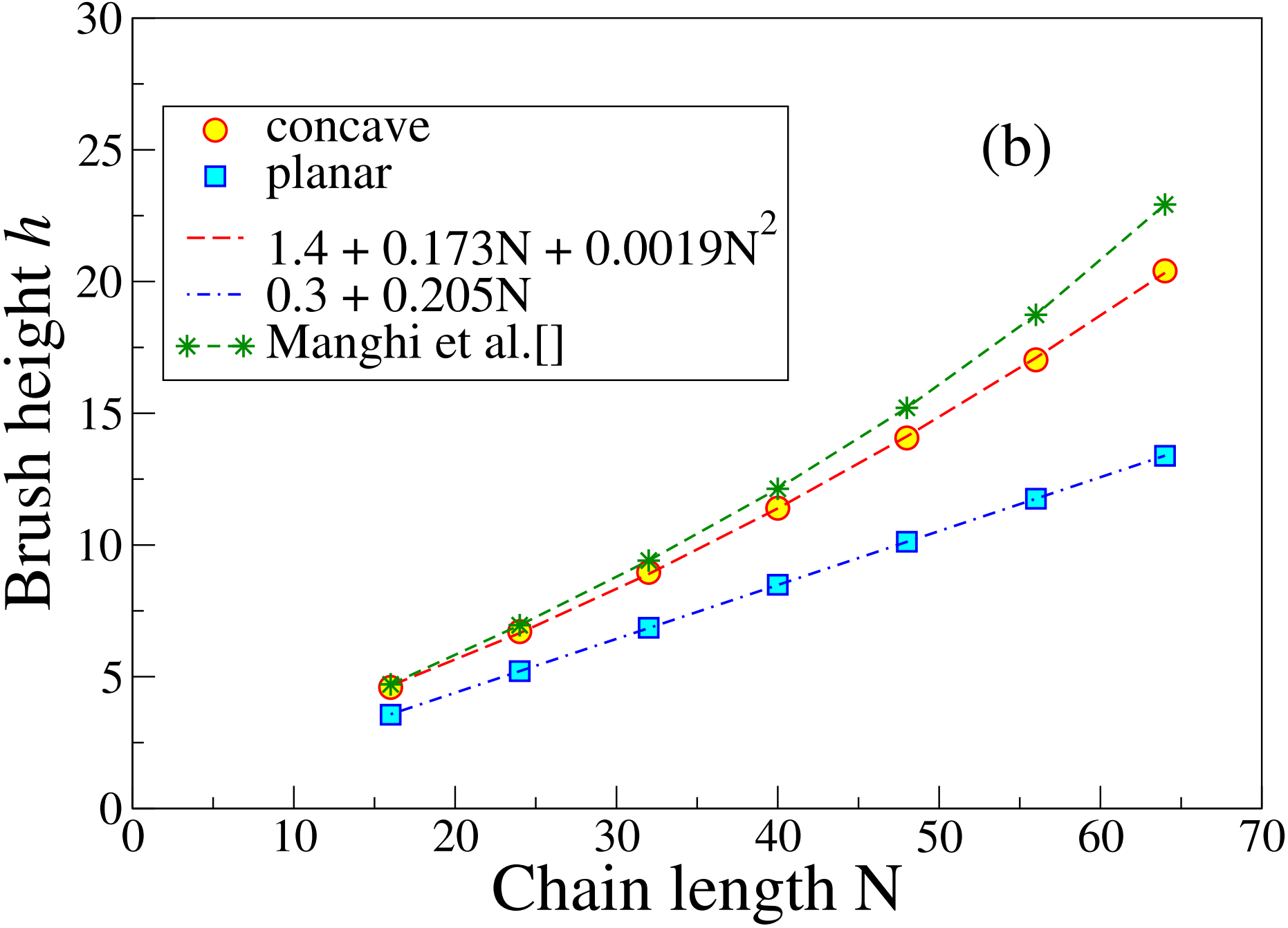
concave
planar
1.4 + 0.173N + 0.0019N^2
0.3 + 0.205N
Manghi et al.[]
(b)
Brush height h
Chain length N
0
5
10
15
20
25
30
0
10
20
30
40
50
60
70

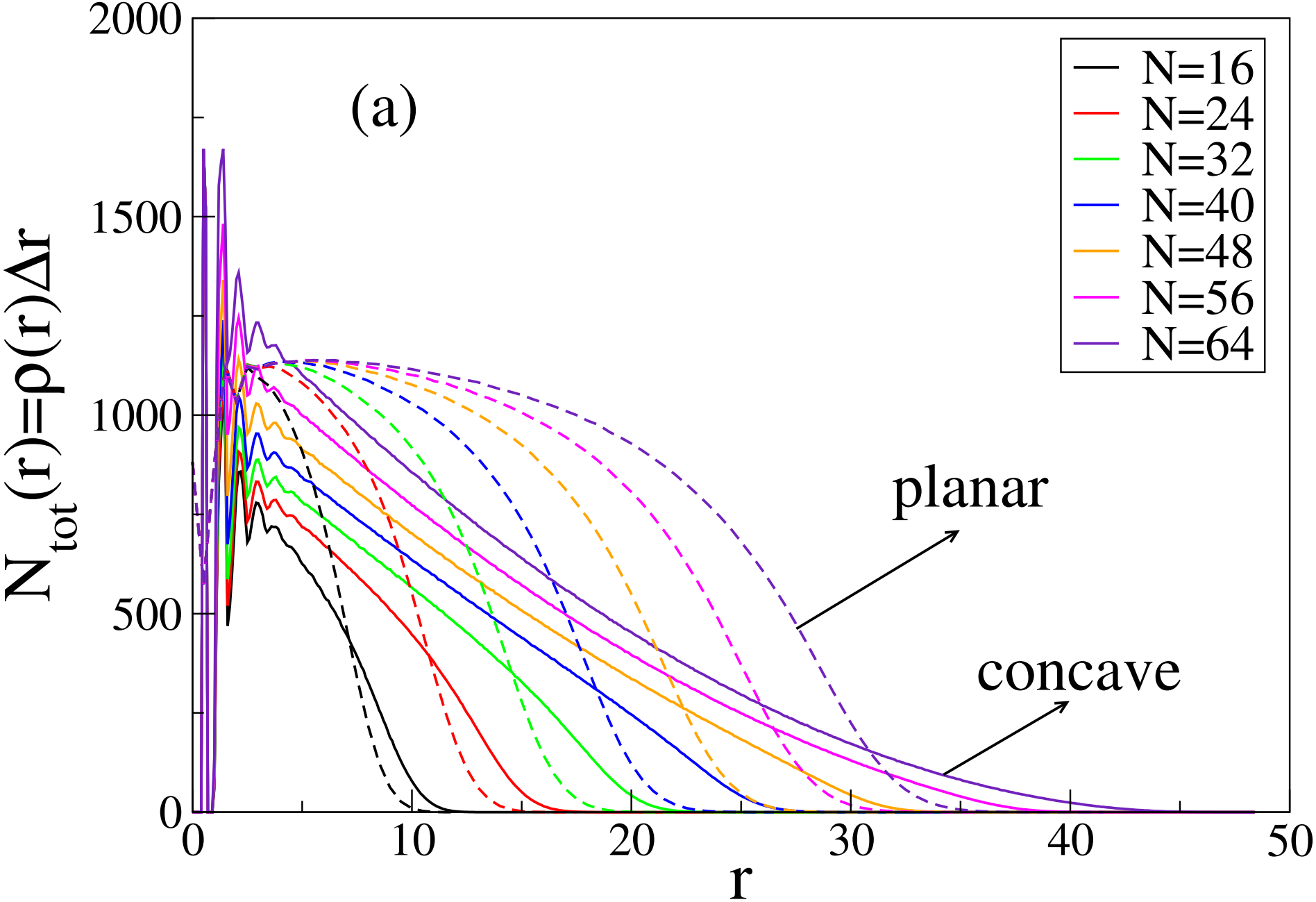
(a)
N=16
N=24
N=32
N=40
N=48
N=56
N=64
planar
concave
$N_{tot}(r)=\rho(r)\Delta r$
r
0
500
1000
1500
2000
0
10
20
30
40
50

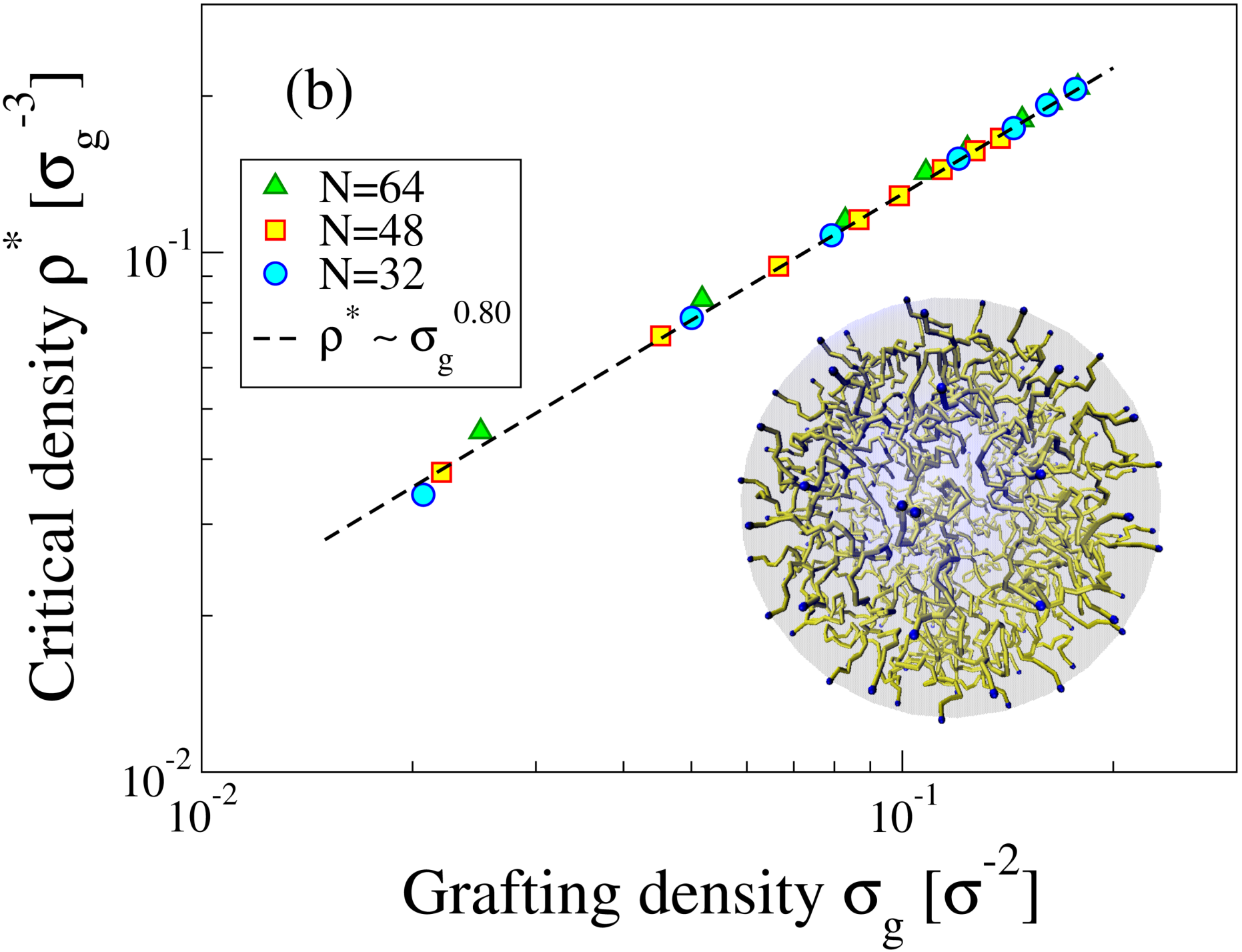
(b)
N=64
N=48
N=32
$\rho^* \sim \sigma_g^{0.80}$
Critical density ρ^* [σ_g^{-3}]
Grafting density σ_g [σ^{-2}]
10^{-1}
10^{-2}
10^{-2}
10^{-1}

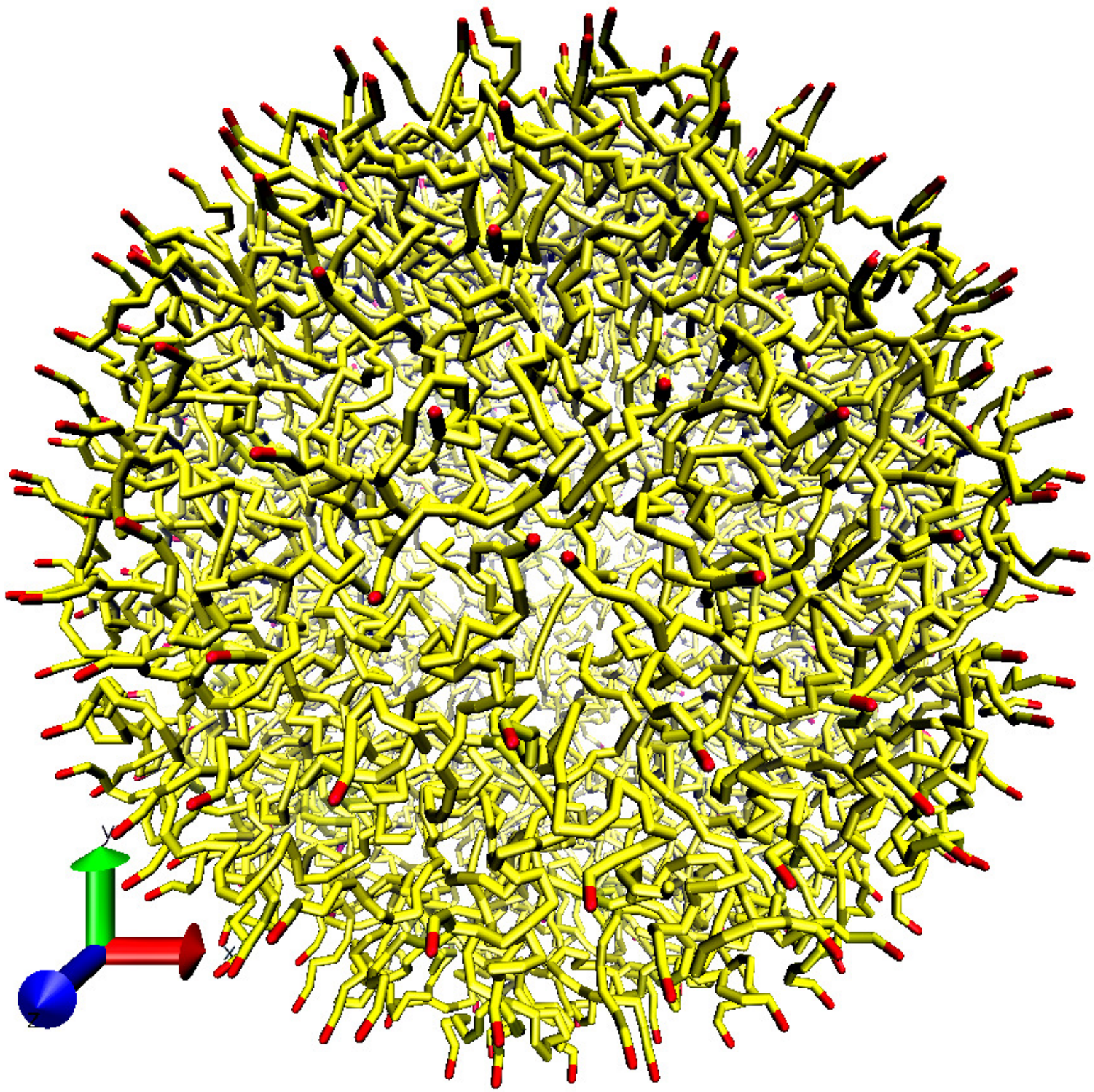
y
x
z

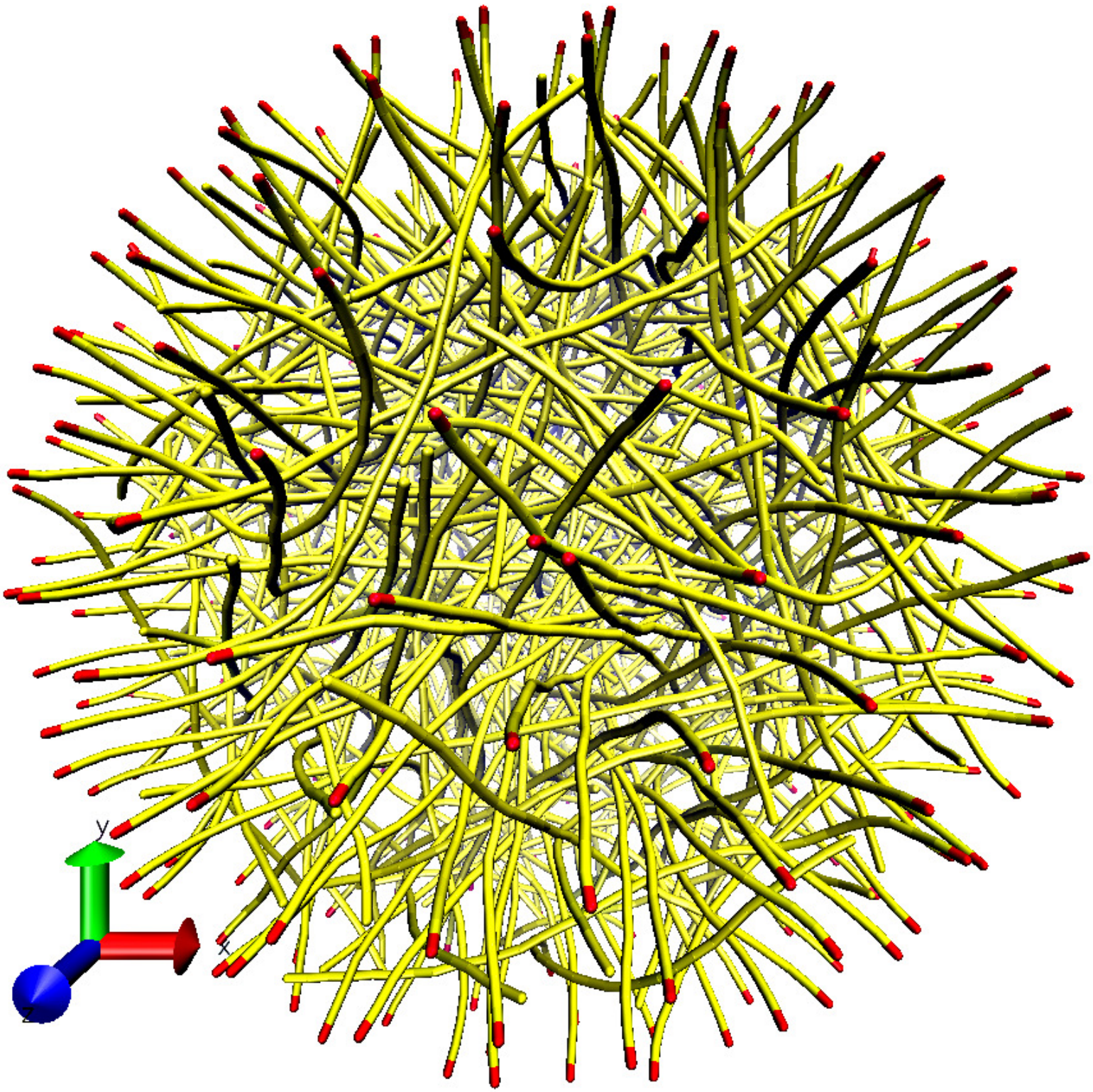
y
x
z

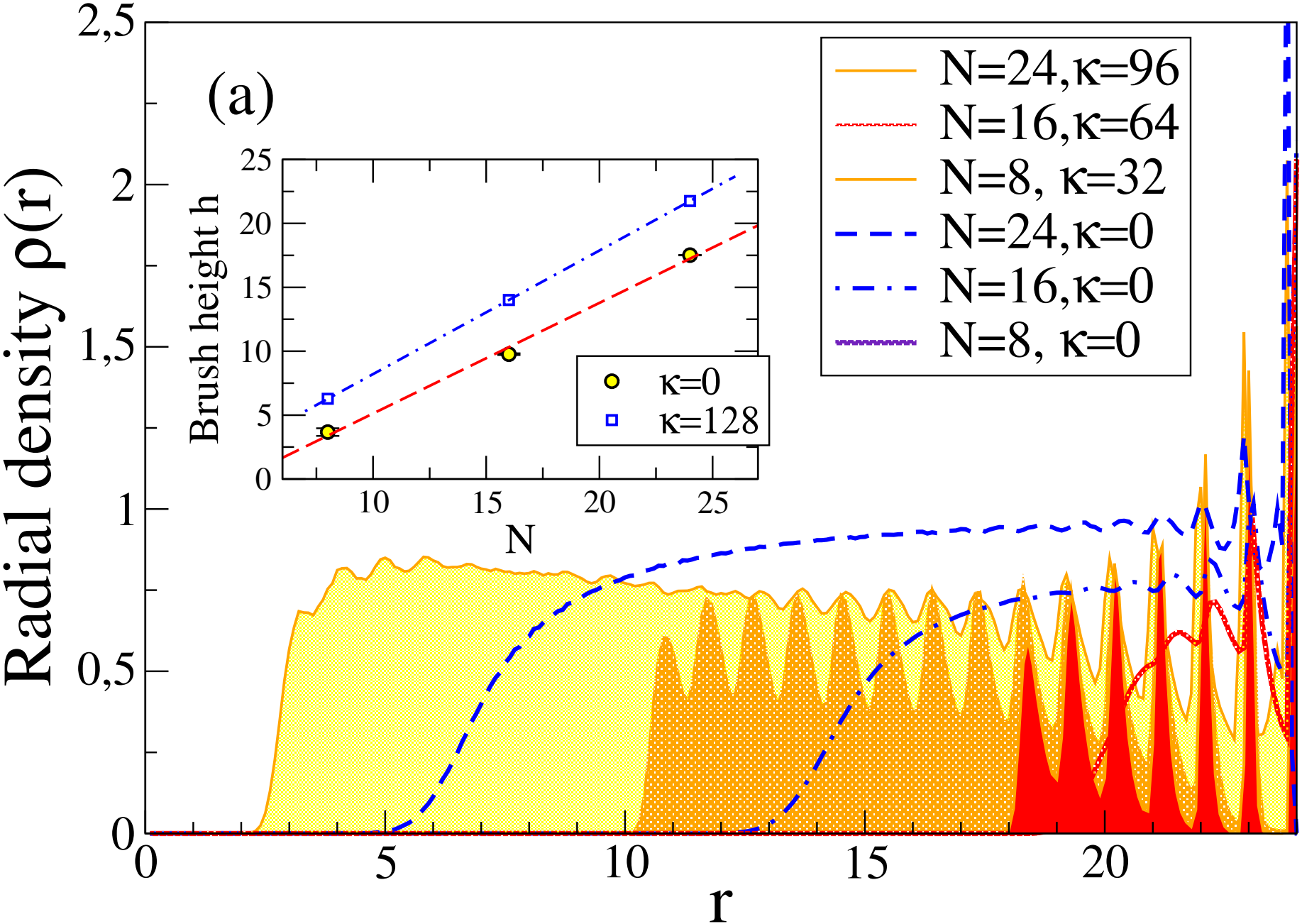
(a)
Radial density ρ(r)
r
N=24,κ=96
N=16,κ=64
N=8, κ=32
N=24,κ=0
N=16,κ=0
N=8, κ=0
Brush height h
N
κ=0
κ=128

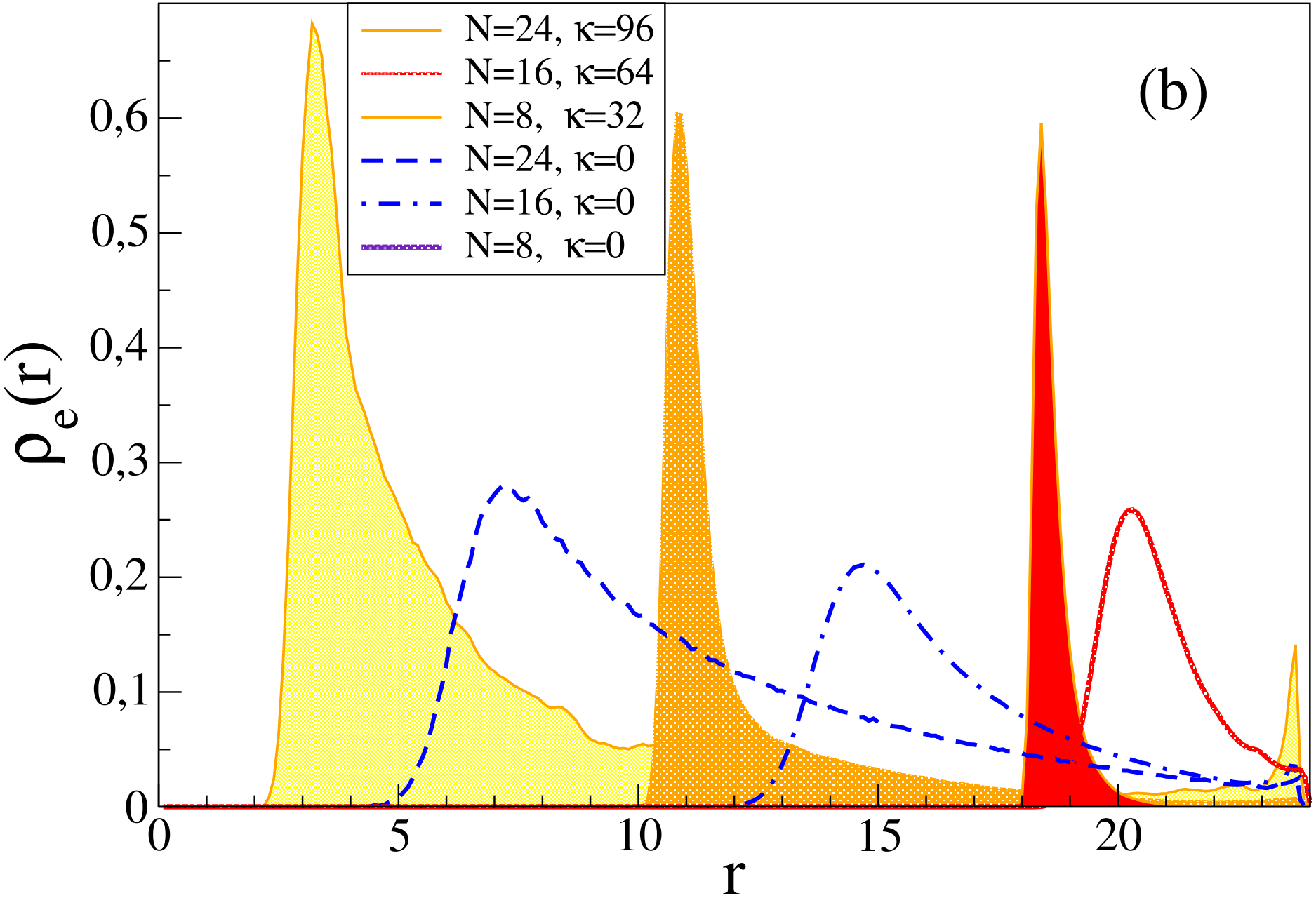
N=24, κ=96
N=16, κ=64
N=8, κ=32
N=24, κ=0
N=16, κ=0
N=8, κ=0
(b)
ρe(r)
r
0
0,1
0,2
0,3
0,4
0,5
0,6
0
5
10
15
20

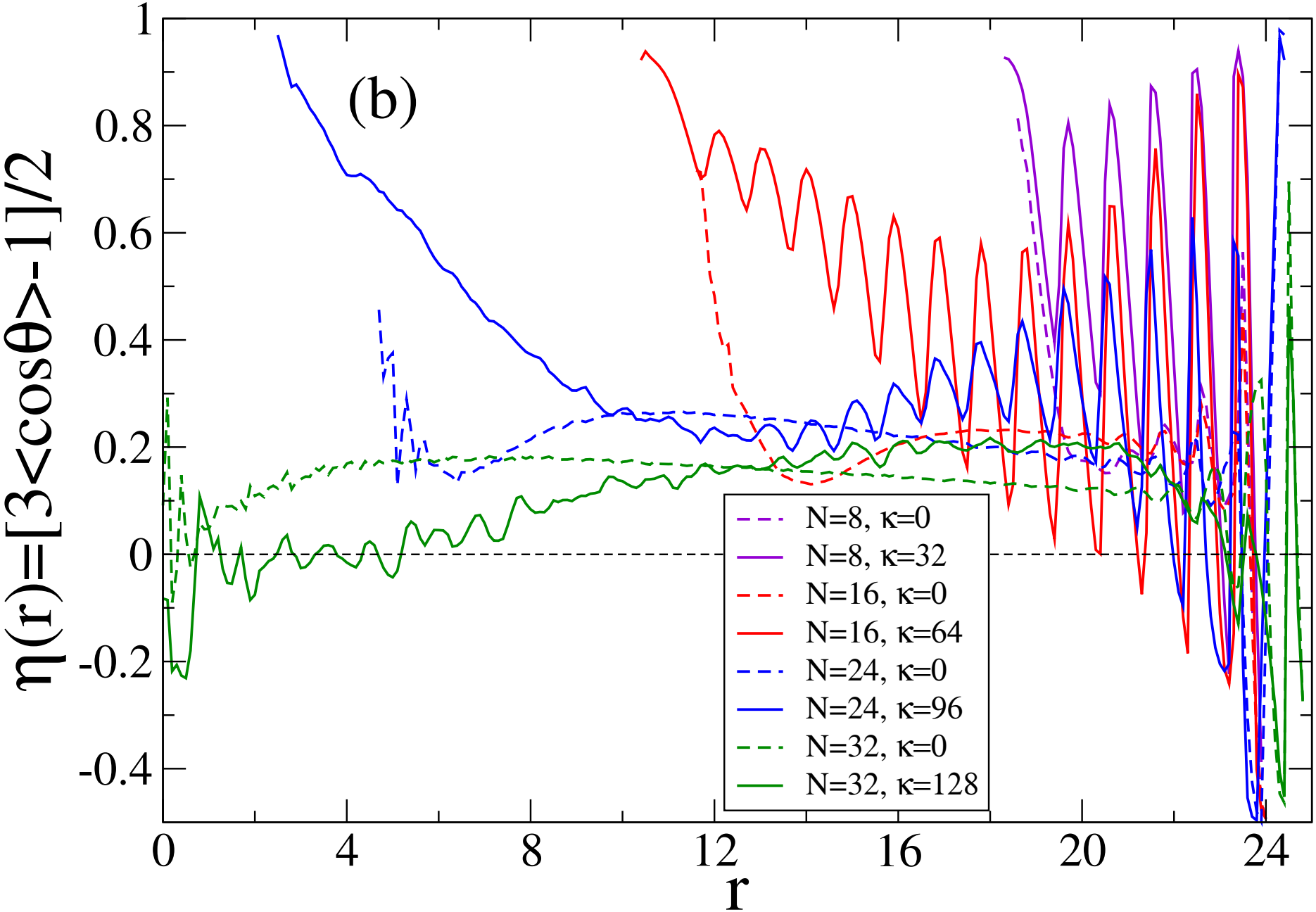
(b)
η(r)=[3<cosθ>-1]/2
r
1
0.8
0.6
0.4
0.2
0
-0.2
-0.4
0
4
8
12
16
20
24
N=8, κ=0
N=8, κ=32
N=16, κ=0
N=16, κ=64
N=24, κ=0
N=24, κ=96
N=32, κ=0
N=32, κ=128

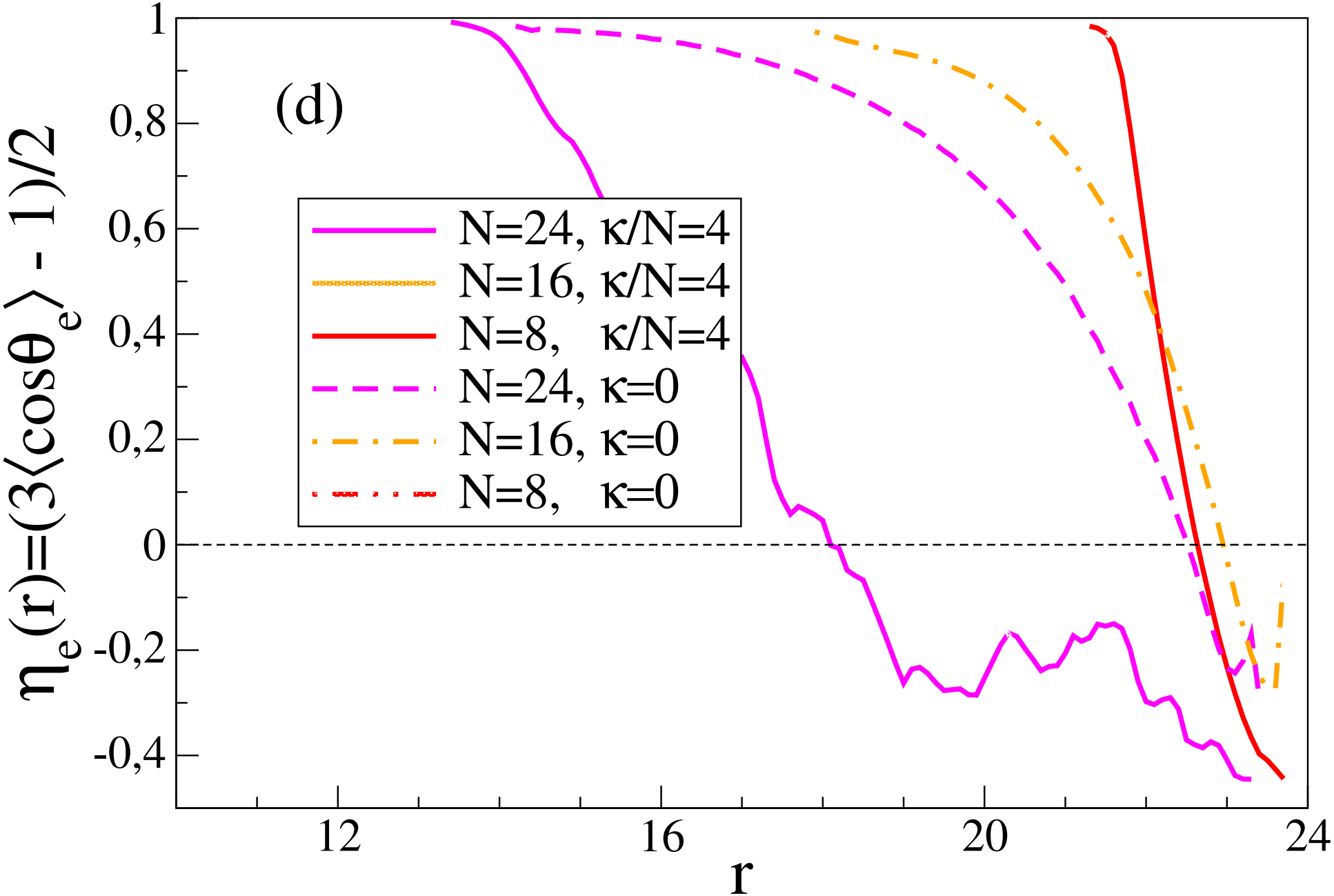
(d)
N=24, κ/N=4
N=16, κ/N=4
N=8, κ/N=4
N=24, κ=0
N=16, κ=0
N=8, κ=0
$\eta_e(r)=(3\langle\cos\theta_e\rangle - 1)/2$
r
1
0,8
0,6
0,4
0,2
0
-0,2
-0,4
12
16
20
24

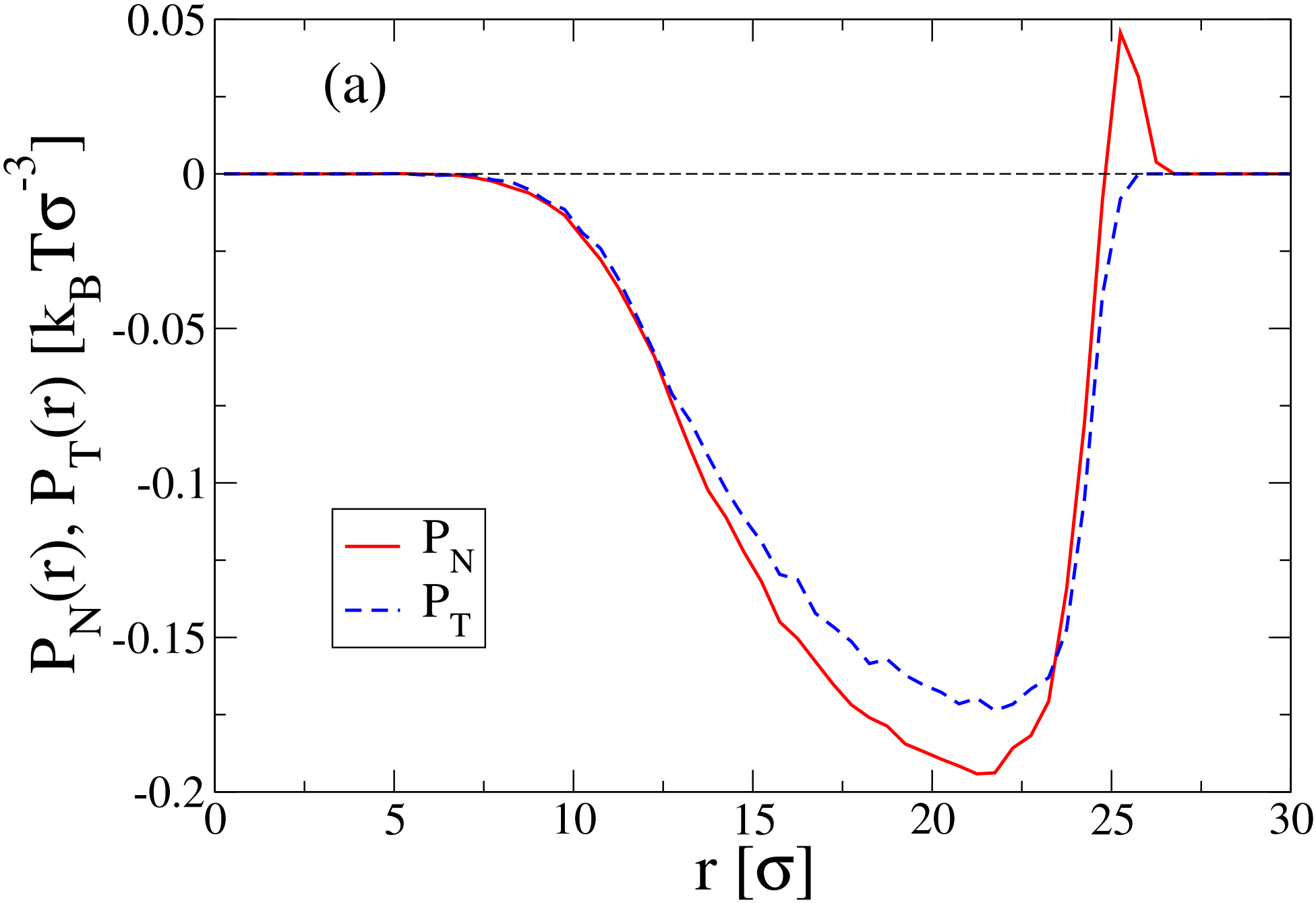
(a)
$P_N(r), P_T(r)\ [k_B T\sigma^{-3}]$
$r\ [\sigma]$
P_N
P_T
0.05
0
-0.05
-0.1
-0.15
-0.2
0
5
10
15
20
25
30

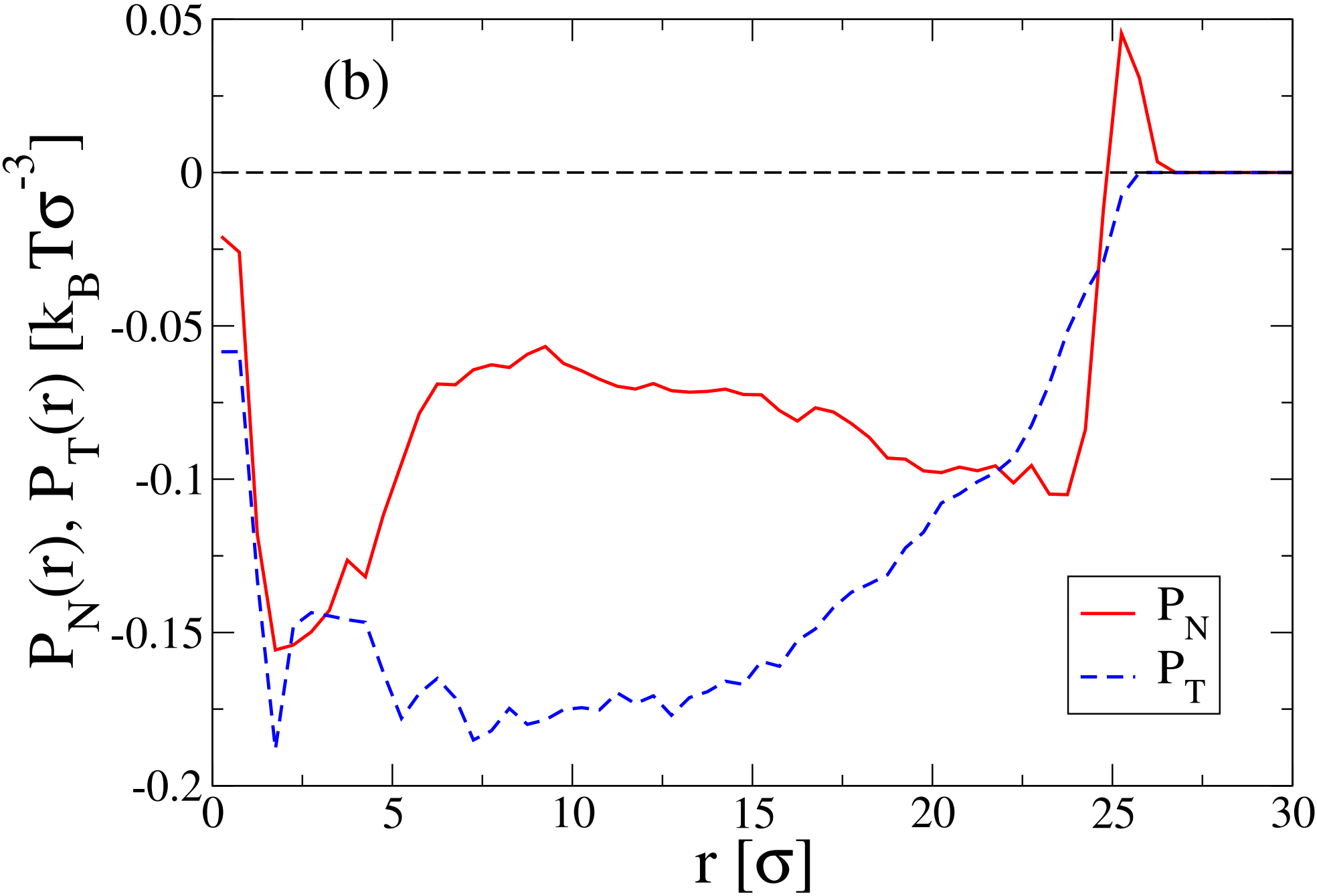
(b)
0.05
0
-0.05
-0.1
-0.15
-0.2
0
5
10
15
20
25
30
r [σ]
P_N(r), P_T(r) [k_B T σ^-3]
P_N
P_T

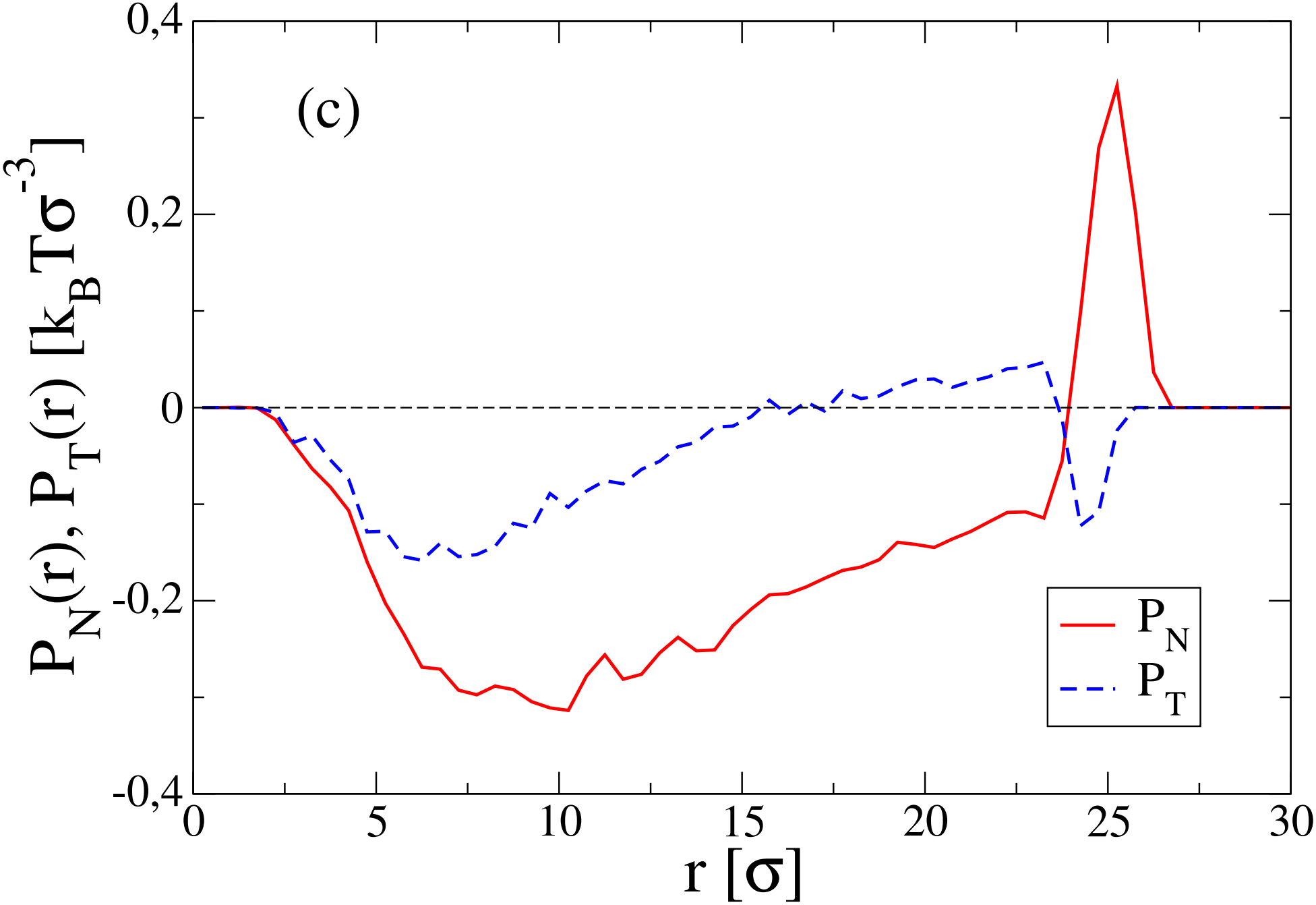
(c)
0,4
0,2
0
-0,2
-0,4
0
5
10
15
20
25
30
r [σ]
P_N(r), P_T(r) [k_B T σ^-3]
P_N
P_T

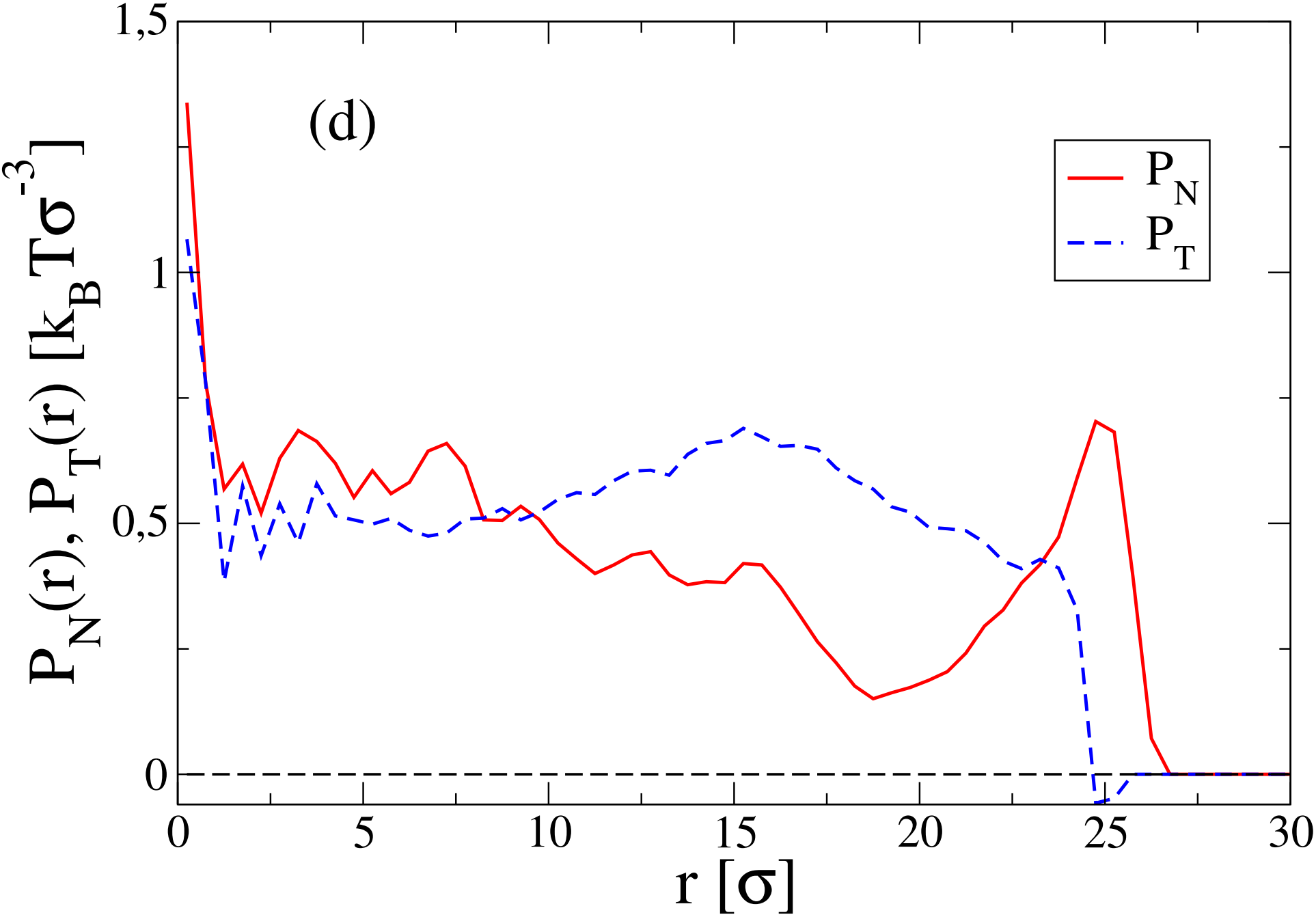
(d)
P_N
P_T
$P_N(r)$, $P_T(r)$ [$k_B T\sigma^{-3}$]
r [σ]
1,5
1
0,5
0
0
5
10
15
20
25
30

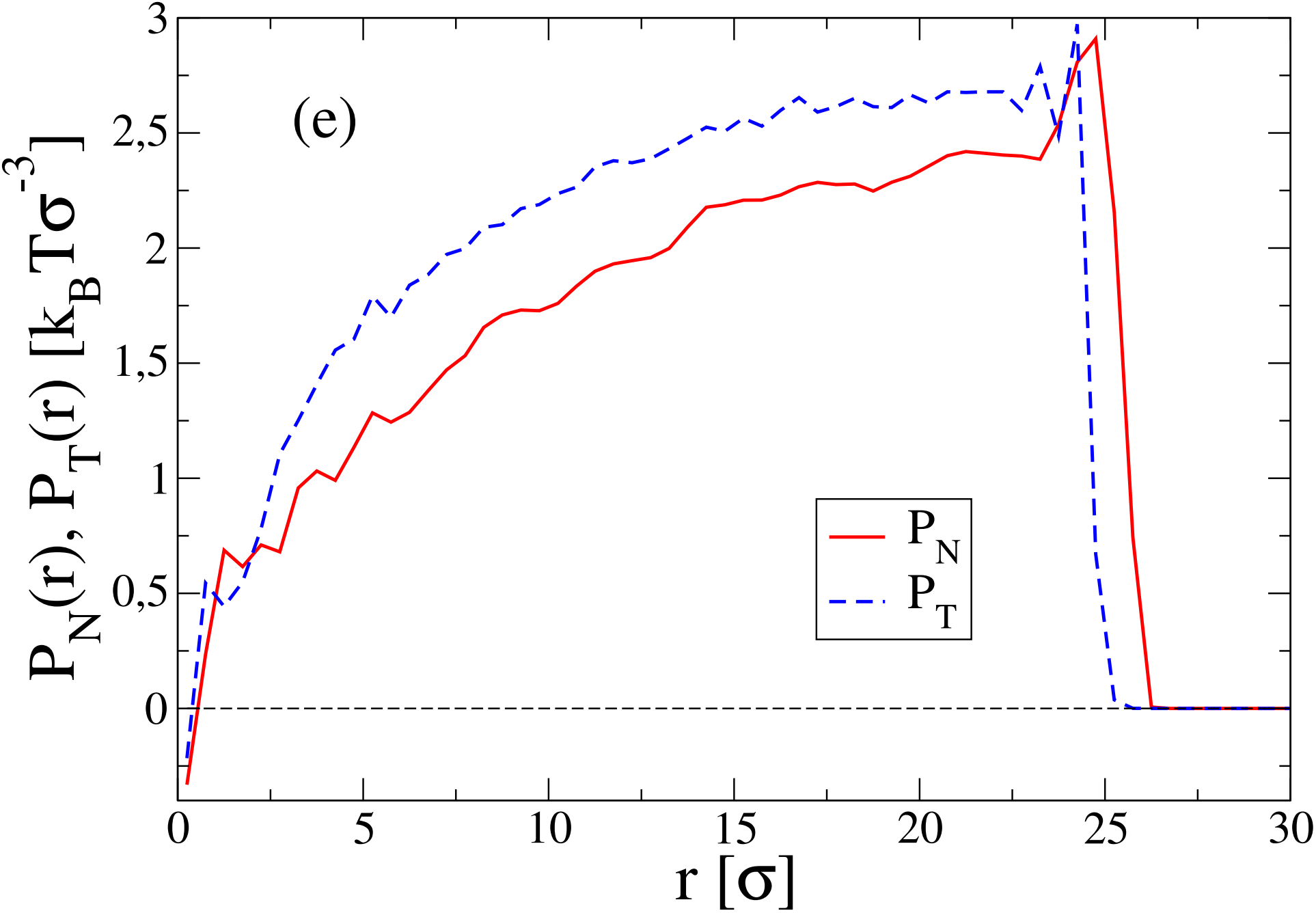
(e)
$P_N(r), P_T(r)\ [k_B T\sigma^{-3}]$
$r\ [\sigma]$
P_N
P_T
0
0,5
1
1,5
2
2,5
3
0
5
10
15
20
25
30

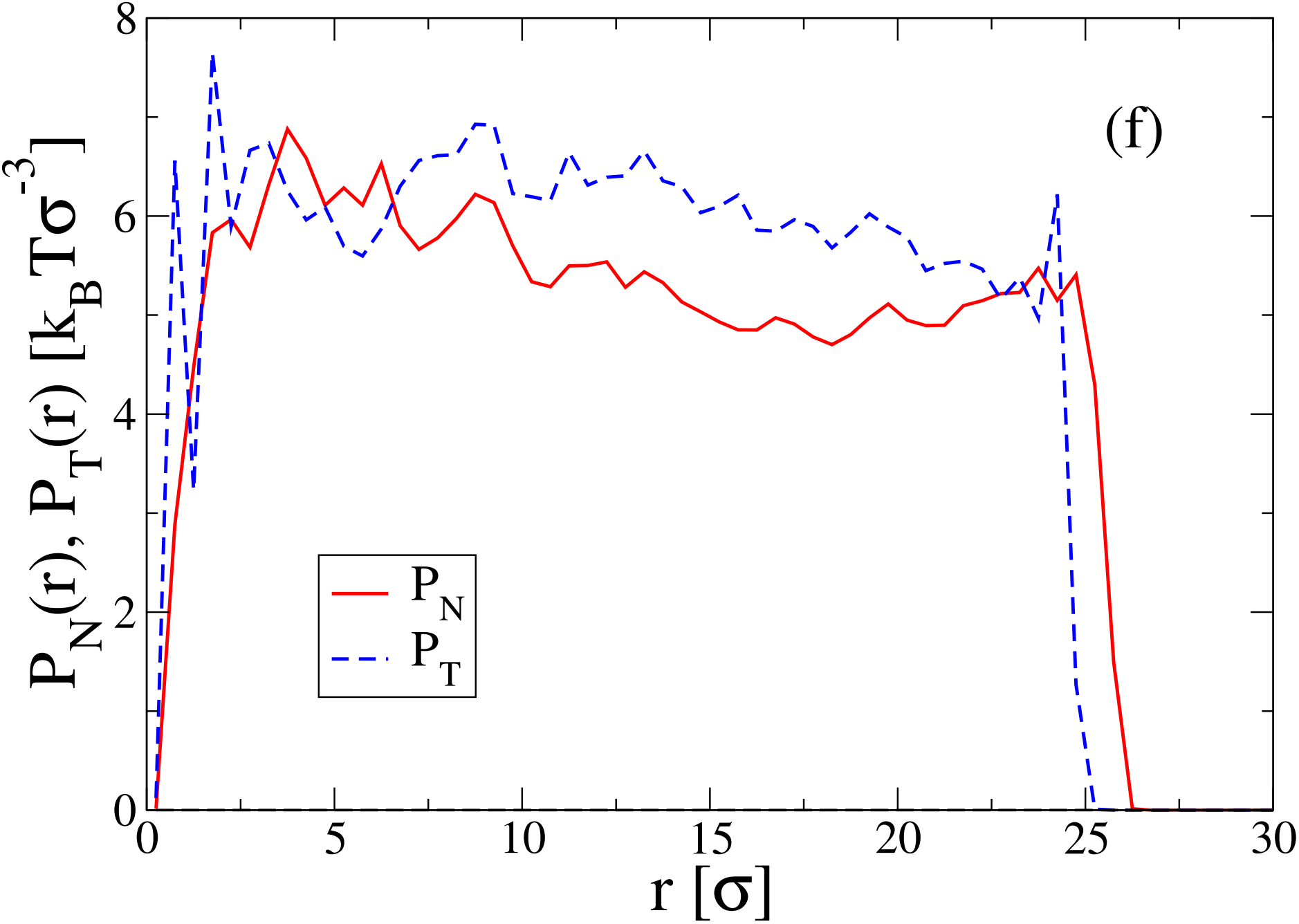
(f)
$P_N(r)$, $P_T(r)$ [$k_B T\sigma^{-3}$]
r [σ]
P_N
P_T
0
2
4
6
8
0
5
10
15
20
25
30

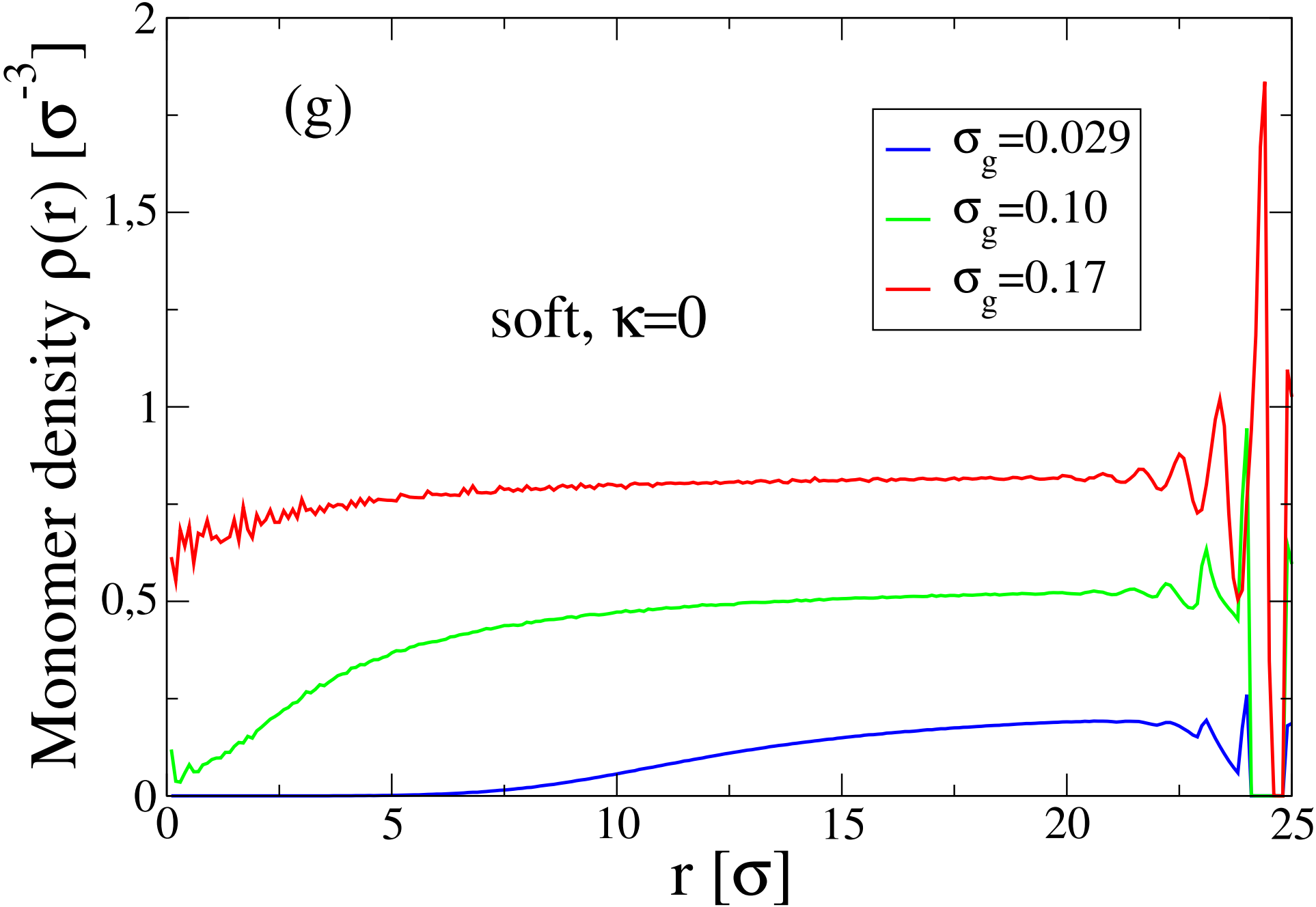
(g)
soft, κ=0
σg=0.029
σg=0.10
σg=0.17
Monomer density ρ(r) [σ-3]
r [σ]
0
0,5
1
1,5
2
0
5
10
15
20
25

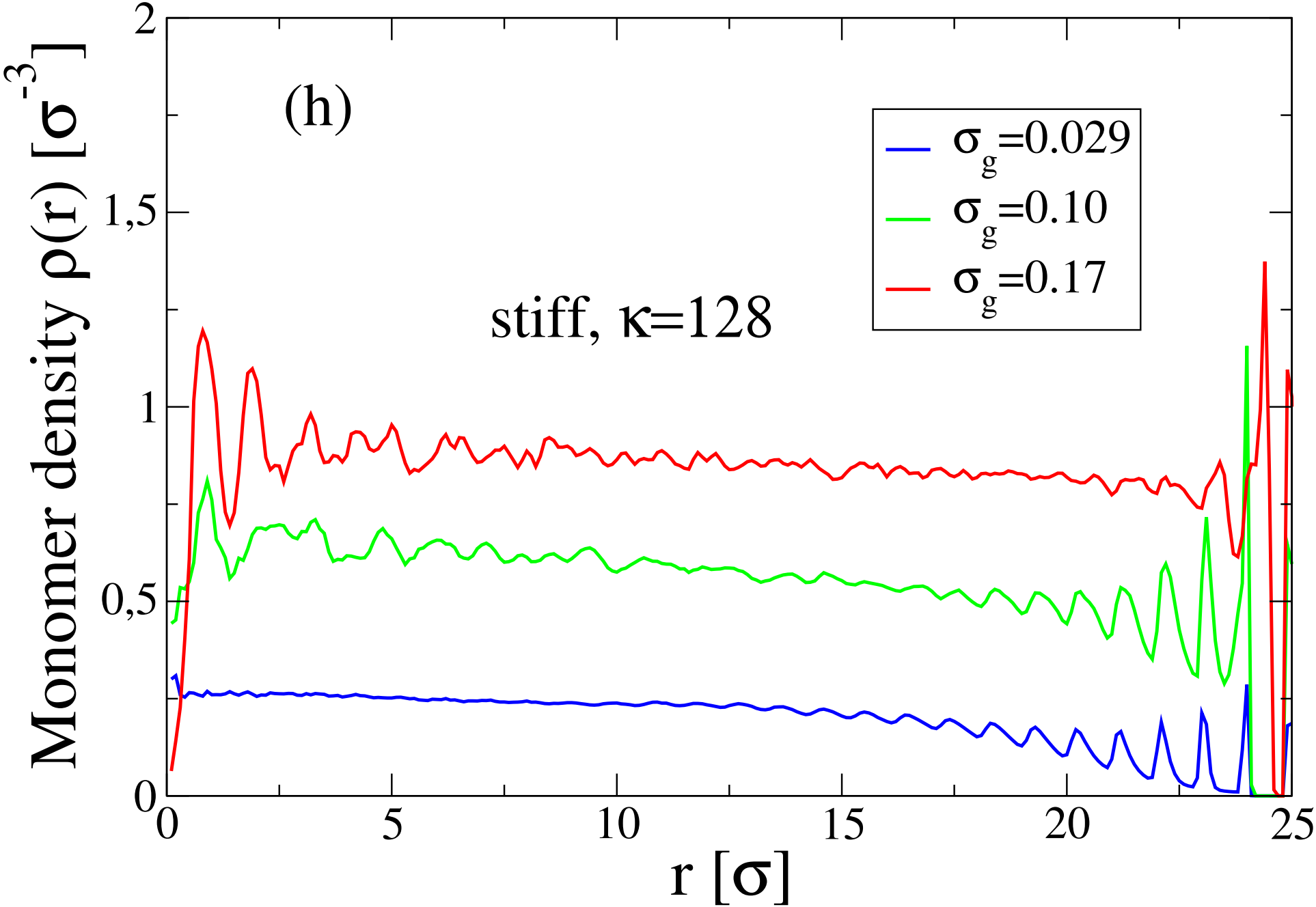
(h)
stiff, κ=128
σg=0.029
σg=0.10
σg=0.17
Monomer density ρ(r) [σ-3]
r [σ]
0
0,5
1
1,5
2
0
5
10
15
20
25

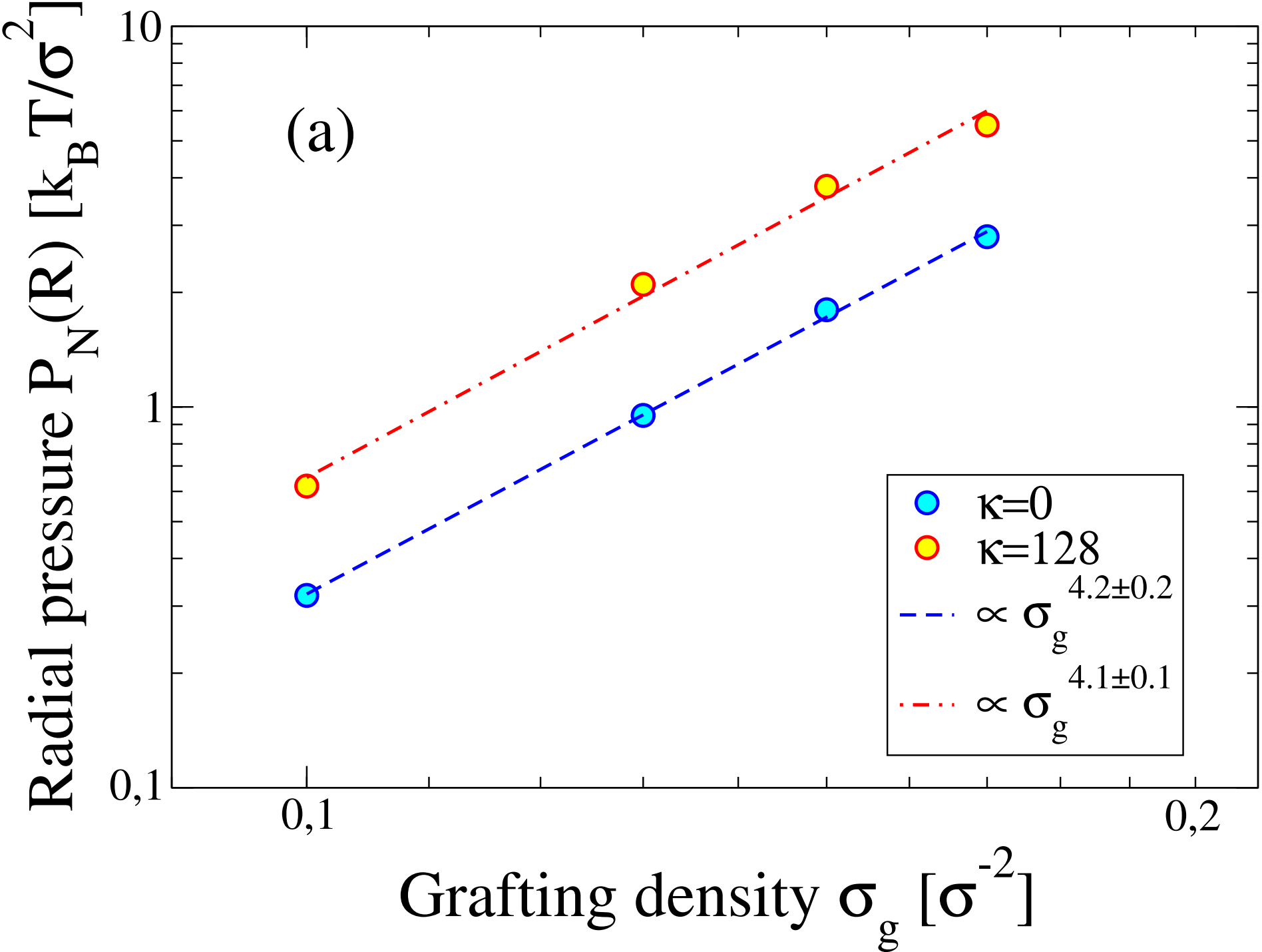
(a)
Radial pressure $P_N(R)$ $[k_BT/\sigma^2]$
Grafting density σ_g $[\sigma^{-2}]$
10
1
0,1
0,1
0,2
κ=0
κ=128
$\propto \sigma_g^{4.2\pm0.2}$
$\propto \sigma_g^{4.1\pm0.1}$

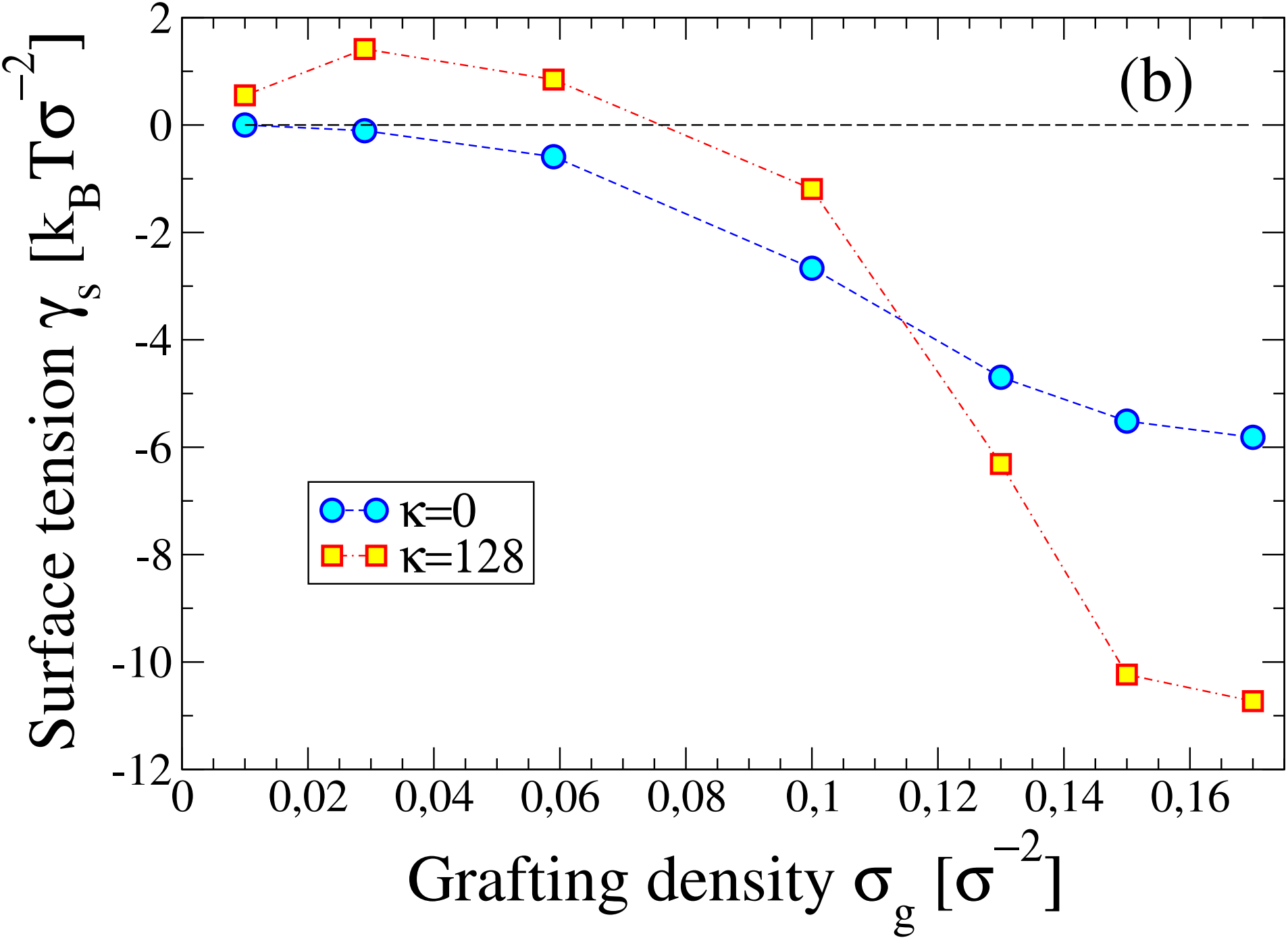
(b)
Surface tension γ_s [$k_BT\sigma^{-2}$]
Grafting density σ_g [σ^{-2}]
κ=0
κ=128
2
0
-2
-4
-6
-8
-10
-12
0
0,02
0,04
0,06
0,08
0,1
0,12
0,14
0,16